LEVEL II

12

PARTICLE IMPACT DAMAGE IN CERAMICS

Final Technical Report

April 1981

By: D. A. Shockey and J. H. Giovanola

Prepared for:

OFFICE OF NAVAL RESEARCH
800 N. Quincy Street
Arlington, VA 22217

Attention: Dr. R. C. Pohanka

Contract No. N00014-76-C-0657
Contract Authority No. NR 023-563/2-02-79 (471)

SRI Project PYU 4928

SRI International
333 Ravenswood Avenue
Menlo Park, California 94025
(415) 326-6200
Cable: SRI INTL MPK
TWX: 910-373-1246

UNCLASSIFIED

SECURITY CLASSIFICATION OF THIS PAGE (When Data Entered)

REPORT DOCUMENTATION PAGE

READ INSTRUCTIONS BEFORE COMPLETING FORM

1. REPORT NUMBER
2. GOVT ACCESSION NO. AD A099693
3. RECIPIENT'S CATALOG NUMBER

4. TITLE (and Subtitle)
(6) PARTICLE IMPACT DAMAGE IN CERAMICS.

5. TYPE OF REPORT & PERIOD COVERED (9)
Final Report.
8 Feb 76 — 7 Feb 81

6. PERFORMING ORG. REPORT NUMBER
PYU 4928

7. AUTHOR(s)
(10) D. A. Shockey, J. H. Giovanola

8. CONTRACT OR GRANT NUMBER(s) (15)
N00014-76-C-0657

9. PERFORMING ORGANIZATION NAME AND ADDRESS
SRI International
333 Ravenswood Avenue
Menlo Park, CA 94025

10. PROGRAM ELEMENT, PROJECT, TASK AREA & WORK UNIT NUMBERS
NR 032-563/2-02-79(471)

11. CONTROLLING OFFICE NAME AND ADDRESS (11)
Office of Naval Research
800 N. Quincy Avenue
Arlington, VA 22217

12. REPORT DATE
April 1981

13. NUMBER OF PAGES
66

14. MONITORING AGENCY NAME & ADDRESS (if different from Controlling Office)
Dr. R. C. Pohanka
Office of Naval Research
800 N. Quincy Street
Arlington, VA 22217
(12) 66

15. SECURITY CLASS (of this report)
UNCLASSIFIED

15a. DECLASSIFICATION/DOWNGRADING SCHEDULE

16. DISTRIBUTION STATEMENT (of this Report)
Approved for public release; distribution unlimited.

17. DISTRIBUTION STATEMENT (of the abstract entered in Block 20, if different from Report)

18. SUPPLEMENTARY NOTES

19. KEY WORDS (Continue on reverse side if necessary and identify by block number)
Si_3N_4, ZnS, Si_3N_4-20%ZrO_2, Al_2O_3-xZrO_2, particle impact, fracture damage, effect of temperature, transformation toughening, predictive capability, stress field history computation, fracture model, crack nucleation, crack growth, residual stresses.

20. ABSTRACT (Continue on reverse side if necessary and identify by block number)
A brief summary is given of the research performed during the first four years of a program investigating particle impact damage in ceramics; a detailed account is given of the research performed during the fifth and final year.

In the first four years, hot-pressed and reaction-bonded silicon nitride, chemical-vapor-deposited zinc sulfide, and a microstructurally toughened ceramic (Si_3N_4-20%ZrO_2) were impacted with tungsten carbide spheres 0.4 mm

DD FORM 1 JAN 73 1473 EDITION OF 1 NOV 65 IS OBSOLETE

UNCLASSIFIED

SECURITY CLASSIFICATION OF THIS PAGE (When Data Entered)

410281

to 2.4 mm in diameter at various velocities. Damage morphologies were ascertained and the fracture damage was assessed quantitatively. Plate impact experiments were performed on ZnS to investigate crack nucleation and growth under uniform dynamic stress fields. Effects of temperature on fracture damage in hot-pressed Si_3N_4 were examined. A finite difference code was used to compute the stress field history in the vicinity of an impact, a computational fracture model was outlined, and development of a predictive capability for particle impact damage was begun.

In the fifth and final year, effects of chemical and phase composition on particle impact damage in $Al_2O_3 \cdot xZrO_2$ ceramics were investigated. Results of quantitative assessment of the fracture damage suggest that retention of the tetragonal phase improves the impact resistance of sintered $Al_2O_3 \cdot xZrO_2$ ceramics and that the improvement is attributable to surface compressive residual stresses.

CONTENTS

LIST OF ILLUSTRATIONS

LIST OF ILLUSTRATIONS (concluded)

LIST OF TABLES

PREFACE

During the five-year course of this research program, a number of specific problems were addressed in the area of particle impact damage in ceramic materials. This final report summarizes briefly the results obtained during the initial four years of the program (details can be found in the four annual reports) and provides a detailed account of the work performed in this fifth and final year.

This research program was initiated by Dr. A. M. Diness and continued by Dr. R. C. Pohanka of the Office of Naval Research. The CVD ZnS material was provided by Dr. James Pappis of the Raytheon Corporation and Mr. Lawrence Kopell of the Air Force Materials Laboratory. Dr. F. F. Lange of Rockwell International provided the microstructurally toughened silicon nitride and aluminum oxide materials.

Our colleagues at SRI International who contributed to the program include R. L. Burback, D. R. Curran, K. C. Dao, D. C. Erlich, Y. M. Gupta, D. J. Rowcliffe, and L. Seaman. Dr. Giovanola performed the research described in Section III through VII of this report.

Other participating technical personnel include R. W. Gates, L. B. Hall, and K. Hirschberg, who assisted in designing the particle accelerator; D. J. Petro, J. C. Terry, M. Menting, and E. Farley, who assisted in posttest examination of impact damage; and B. Lew and S. L. McHugh, who helped with data reduction. W. J. Murri, A. Urweider, A. Bartlett, and A. J. Baggett assisted in conducting the plate impact experiments.

I INTRODUCTION

Materials having acceptable radiation transmission properties for use as infrared windows and radomes on aircraft generally have poor resistance to fracture in particle impact situations. The microfractures that form and grow under bombardment by rain, dust, and ice particles scatter incident radiation and result in continuous degradation of the optical properties with flight time. Longer exposures or more severe impact environments can result in interaction of microfractures with each other and with the radome surfaces, causing mass loss (erosion) and gross mechanical failure. Erosion and gross failure behavior at high temperature must also be considered in designing ceramic components of turbine engines. The Navy wishes to ascertain high temperature failure mechanisms, to establish more impact-resistant microstructural forms of ceramic materials, and to develop a capability for predicting the fracture behavior. In support of these needs, SRI International performed research to understand failure behavior of ceramics at room temperature and at turbine engine operating temperatures, to examine failure behavior of microstructurally toughened ceramics, and to establish expressions and material properties governing fracture development in ceramic window, radome, and engine materials under hard particle impact.

Section II of this final report summarizes the research performed during the first four years of this program.* Main goals were to establish expressions, properties, and a predictive capability for impact-induced fracture, and to investigate particle impact damage in Si_3N_4.

The balance of the report, Sections III through VII, describes the work performed during this fifth research year. Main goals were to evaluate the impact resistance of transformation-toughened ceramics, and to investigate the mechanism(s) responsible for any improvements.

*Details are given in the four annual reports.

II SUMMARY OF PREVIOUS WORK ACCOMPLISHED UNDER PRESENT CONTRACT

Expressions, Properties, and a Predictive Capability for Impact-Induced Fracture

A primary objective of the SRI program was to establish expressions and material properties governing fracture development in ceramic window, radome, and engine materials under hard particle impact. If such expressions and properties can be established, they can be used to predict such engineering quantities as optical and mechanical lifetimes under specified impact environments. Furthermore, they can be useful in guiding the development of more impact-resistant microstructures by permitting systematic investigation of the effects of compositional and processing variables.

Our approach consisted of the following tasks:

- Establish an experiment that can be analyzed to allow identification and evaluation of the material properties governing resistance of semibrittle materials to fracture damage by particle impact. Experiments having the highest probability of success appeared to be those closely simulating particle impact conditions, but having a simple impact geometry to aid in interpretation and analysis. Thus, we performed experiments involving normal (90°) impact of a single, elastic sphere against a flat specimen surface.

- Obtain an understanding of how fracture damage develops about an impact site. We studied damage phenomenology by performing experiments at various velocities so as to produce various levels of damage ranging from below incipient to surface fragmentation. By examining with a microscope the impact sites and cross sections taken through the sites, we deduced how fracture damage evolves.

- Describe quantitatively the deformation and fracture damage produced by particle impact. Definition of impact erosion properties requires a knowledge of the relationships between loading parameters and material failure response; therefore, a quantitative description of deformation and fracture is required. We counted and measured the radial, ring, and lateral cracks at particle impact sites to obtain crack size distributions for various impact velocities.

- Calculate the stress field histories experienced by material in the vicinity of an impact site or choose an appropriate load parameter for correlation with fracture damage. To extract fundamental and general material properties, the damage quantities should be correlated with the stress or strain histories experienced at the appropriate locations in the impacted specimen. We used a finite difference code to compute stress and strain as a function of location and time for a material undergoing plastic flow but not fracture. We also sought simpler measures of the load for correlation with damage.

- Correlate fracture damage with computed stress field histories or with an appropriate load parameter to extract expressions and properties describing impact damage development. The numbers and sizes of radial cracks when so correlated yield expressions and properties describing crack nucleation and growth.

This approach was carried out on chemical-vapor-deposited zinc sulfide (CVD ZnS). Individual 800-μm-diameter tungsten carbide (WC) spheres were accelerated in a pneumatic gun to velocities up to 80 m/s and made to impact polished surfaces of CVD ZnS to produce various levels of impact damage in the form of a plastic impression and a population of cracks. The size distributions of radial cracks were determined as a function of plastic impression radius. The shapes of the crack size distribution curves suggest that the size distribution of inherent flaws is exponential, consistent with the results of probability theory. These curves further suggest that the growth law for radial cracks is similar in form to expressions derived from elastic energy balances.

Material properties describing the development of radial cracks were obtained by correlating the crack size distributions with plastic impression strain. These parameters included threshold strains and characteristic rates for crack nucleation and growth. The effects of particle size, shape, and loading rate on fracture damage were investigated by performing experiments in which 400- and 800-μm-diameter tungsten carbide spheres and cylinders were impacted and quasi-statically pressed onto polished CVD ZnS surfaces. Comparison of the crack size distributions indicated significant particle size effects, but lesser effects from loading rate.

The crack nucleation and growth parameters for the cases of impacts and indents with 400- and 800-μm-diameter spheres were determined. However, discrepancies among the parameter values suggest that a simple load parameter such as plastic impression strain may be inappropriate for extracting erosion properties. Therefore, a detailed computation of the stress field history was undertaken.

A two-dimensional Lagrangian, finite difference, wave propagation code, TROTT, was provided with a slide line capability and used to simulate the impact of an 800-μm-diameter WC sphere and a ZnS plate at velocities of 5, 30, and 60 m/s. Plastic flow was allowed to occur according to an experimentally determined stress-strain relation, but cracking and the associated stress relaxation were not treated in these initial calculations. The computation simulated qualitatively all of the important aspects of a particle impact event, and gave good quantitative agreement with experimental measurements of rebound velocity and crater dimensions.

Mathematical expressions that describe crack development in ZnS under particle impact load histories were deduced from observations of the number and sizes of radial cracks produced by impact at various velocities. These expressions treat damage development as a crack nucleation and growth phenomenon and constitute a computational fracture model that, written as a subroutine, can be used in conjunction with the wave propagation code to calculate the extent of fracture damage resulting from a given particle impact. The parameters in the model, because they are material-specific and hence act as dynamic fracture properties, can be used to rank and evaluate candidate materials for various impact erosion applications.

Objectives of future work should be to establish the functional form of the crack nucleation expression, to incorporate the fracture model in the wave propagation code, and to simulate computationally selected particle impact experiments.

Particle Impact Damage in Silicon Nitride

Silicon nitride has many of the properties required of materials for gas turbine applications. High strength at elevated temperatures, low

density, low coefficient of thermal expansion, and high oxidation resistance make silicon nitride an attractive low-cost alternative to refractory alloys for stators, rotors, and other high temperature engine components. Furthermore, silicon nitride is a candidate for radomes. A major concern in using any ceramic in applications where impact by flying particles is encountered is the relatively high (compared to metals) susceptibility to surface damage and subsequent brittle fracture.

For these reasons, the response of silicon nitride materials to particle impact is of interest to the Navy and hence was investigated in this program. In the following paragraphs, we summarize our findings on hot-pressed and reaction-bonded grades of Si_3N_4 and briefly describe the impact behavior of Si_3N_4 that was toughened by the addition of ZrO_2. Using the pneumatic gun mentioned in the previous subsection, we accelerated WC spheres against Si_3N_4 plates to establish damage morphologies, ascertain threshold conditions for the various fracture modes, and observe damage development at conditions above threshold. We also investigated effects of particle size, oxide scale, and loading rate on damage response.

Fracture damage in fully dense HP Si_3N_4 began with the formation of shallow ring crack segments that increased in number and size with increasing impact velocity. At successively higher velocities, Hertzian cone cracks, a plastic impression, and about five radial cracks formed. At still higher velocities, lateral and median-vent cracks were produced and the number of large radials increased to a maximum of about 8 or 9. Interaction of these crack types with each other and with the specimen surface occurred at approximately 231 m/s and resulted in erosion. The damage thresholds are summarized in Table 1.

The presence of an oxide scale (roughly 20 μm thick) had little influence on the morphology and extent of fracture damage in HP Si_3N_4. However, the oxide layer spalled easily at low impact velocities, suggesting higher erosion rates for Si_3N_4 in oxidizing environments.

The damage phenomenology in 85% dense, reaction-bonded (RB) Si_3N_4 was similar to that in the hot-pressed material. However, for RB Si_3N_4, ring cracking and all subsequent stages of the damage process began at roughly two-thirds the stress needed to produce damage in HP Si_3N_4 (Table 1).

Table 1.
DAMAGE THRESHOLDS FOR SILICON NITRIDE

Si_3N_4 Material	Sphere Characteristics		Ring Cracking		Plastic Deformation		Sphere Failure	
	Material	Diameter (mm)	Impact Velocity (m/s)	Tensile Stress (GPa)	Impact Velocity (m/s)	Compressive Stress (GPa)	Impact Velocity (m/s)	Compressive Stress (GPa)
Hot-Pressed	WC	2.4	17	2.8 (2.9*)	32	28	24	25 (26*)
	WC	1.6	38	2.9	~42	30	46	31
	Steel	2.4	42	3.1	–	30	46	17
Reaction-Bonded	WC	1.6	11	2.0	24	17	>73	>27

*Measured in quasi-static indentation.

A significant effect of particle size was observed, but loading rate effects were small. Decreasing the WC particle diameter by 33% caused roughly a two-fold increase in ring crack threshold velocity (no increase in threshold stress) and a 50% increase in the threshold velocity for plastic impression (a 7% increase in stress).

Fracture damage under quasi-static loading rates appeared to be similar to that under impact loads, and ring cracks were observed at similar load thresholds. However, flow and fracture of the indenting WC spheres prevented application of higher loads and hence production of further specimen damage.

An elastic Hertzian analysis of the stress field adequately predicted our observations of ring cracking in HP Si_3N_4. In the elastic-plastic regime, however, the measured area of fracture damage was consistently broader than that predicted by elastic theory, indicating that yielding and wave propagation effects must be accounted for.

Impacts of tungsten carbide spheres on hot-pressed Si_3N_4 produced elastic fracture behavior (ring and cone cracks) at room temperature, but elastic-plastic fracture behavior (plastic impressions and radial cracks) at 1400°C. In contrast, no change in fracture pattern at the two temperatures was produced by impact with steel spheres. These results may be explained by the relative abilities of the impacting spheres to cause plastic flow at the impact site and hence to alter the stress distribution in the Si_3N_4 specimens.

The type and extent of damage produced by hard particle impact at 1400°C appears to be more deleterious to structural integrity than that produced at 20°C under equivalent particle impact loading conditions.

When impacted by 1.2-mm-diameter tungsten carbide spheres at velocities to 200 m/s, oxidized Si_3N_4-20 vol% ZrO_2 exhibited decidedly less fracture damage than unoxidized material. The impact velocity necessary to initiate ring and radial cracks was significantly higher for oxidized materials, and the rate at which fracture damage, once nucleated, developed was substantially lower. This enhanced dynamic performance is consistent

with the enhanced quasi-static properties reported by Lange and may involve oxidation-induced compressive surface stresses, oxidation-induced softening, or both.

The impact resistance of transformation-toughened materials, namely the $Al_2O_3 \cdot xZrO_2$ system, was investigated during the fifth research year of this program. The remaining sections of this report detail the procedures and results.

III. BACKGROUND

Transformation-toughened ceramics may well exhibit significant improvements in resistance to particle impact. The tetragonal-to-monoclinic phase transformation made possible by ZrO_2 additions to brittle ceramics, has been shown to enhance their static properties.[1] Significant improvements in fracture toughness and flexural strength (up to 50%) have been reported in the $Al_2O_3 \cdot xZrO_2$ system as compared with the values for pure Al_2O_3. The precise mechanisms by which fracture resistance is increased in these quasi-static situations are, however, not yet adequately understood and research is still under way to determine optimum compositions.

The phase transformation occurs in the following manner. Upon cooling from around 1200°C to room temperature, ZrO_2 undergoes a phase transformation from a tetragonal to a monoclinic structure. The transformation is athermal and diffusionless and involves only a shape change that is associated with a 3% to 5% increase in volume.[2,3] Because of its analogy with transformations encountered in metallic systems, it is termed martensitic.

Retention of tetragonal ZrO_2 in other brittle ceramic systems has been shown to improve their fracture properties significantly.[4-8] The retained tetragonal phase is thought to transform to the monoclinic phase under the elevated stresses at the running crack tip. It plays the role of a toughening agent by increasing the amount of energy absorbed during crack propagation by the amount of strain energy associated with the unconstrained phase transformation.

Recent work by Lange[3,9] has shown that the metastable phase can be retained at lower temperature only if the surrounding matrix exerts a sufficiently high elastic constraint on the tetragonal ZrO_2 particle. Lange further showed that the phase transformation will be influenced by alloying additions (e.g., Y_2O_3, CeO_2) and by the occurrence of microcracking

or microtwinning. He concludes that given the elastic properties of the surrounding matrix, the temperature, and the amount and type of additives, there is a critical ZrO_2 inclusion size below which the martensitic transformation is not energetically favorable. Based on energy considerations, Lange was also able to make predictions about the increase in fracture toughness resulting from the tetragonal-to-monoclinic transformation.

A parallel experimental investigation on composite $Al_2O_3 \cdot xZrO_2$ confirmed Lange's prediction of the improvement in mechanical properties due to the presence of tetragonal ZrO_2.[1] A series of tests on Al_2O_3 samples containing 2 mol% of Y_2O_3 and an increasing volume fraction of ZrO_2 (0-40%) completely in the tetragonal phase indicated an increase in fracture toughness and in flexural strength with increasing amount of ZrO_2. The results showed significant improvement in mechanical properties compared with data from pure Al_2O_3 samples or $Al_2O_3 \cdot xZrO_2$ composites in which the zirconia was in the cubic phase. It was also found that surface abrasion had a beneficial role on the flexural strength of ZrO_2-toughened Al_2O_3, probably because the tetragonal-to-monoclinic transformation of ZrO_2 induced during grinding leaves a surface layer of compressive residual stresses.

The enhanced static properties of these ceramics encouraged us to evaluate their response to particle impact, and to examine in a preliminary way the effects of chemical and phase composition on impact resistance.

IV EXPERIMENTAL

Materials

All specimens used in this investigation were supplied by Dr. F. F. Lange of the Rockwell International Science Center. Two series of specimens were tested. In the first series, the ZrO_2 content was fixed at 30 vol% and the phase composition in four specimens was varied from fully monoclinic to fully tetragonal by the addition of increasing amounts of Y_2O_3 (0.5, 1.0, 1.5, 2.0 mol%, respectively). The precise proportion of tetragonal ZrO_2 in the intermediate specimens was not established. This batch of materials was produced by sintering; the specimens were roughly 30 mm by 15 mm by 5 mm in size. No mechanical property data were available for the sintered materials. The specimens with 0.5 and 1.0 mol% Y_2O_3 were highly cracked;[10] the sintered specimens were also not fully dense.

In the second series, four hot-pressed samples varied in composition from 12.3 to 29.3 vol% ZrO_2, all of which was in the metastable tetragonal phase. These samples were about 20 mm by 4 mm by 4 mm in size and were broken halves of the bend specimens tested in Reference 1. The available mechanical property data for these materials are summarized in Table 2 with values for pure Al_2O_3 given for comparison. All specimens had a ground surface finish corresponding to a 220-grit grinding wheel.

The effect of residual stresses induced by grinding operations was studied by testing two additional specimens that had undergone an annealing heat treatment subsequent to grinding (1300°C for 1 hr). Both had about the same composition, namely 30 vol% ZrO_2 + 2 mol% Y_2O_3, but one was hot-pressed whereas the other was sintered.

Experimental Arrangement and Procedure

The two series of $Al_2O_3 \cdot xZrO_2$ composite ceramics were impacted at various velocities with single tungsten carbide spheres of several sizes

Table 2.
COMPOSITION AND PROPERTIES OF HOT-PRESSED MATERIALS

COMPOSITION (vol% ZrO_2)	DENSITY (g/cm^3)	HARDNESS H (GPa)	TOUGHNESS K_c (MPa $m^{1/2}$)
0	3.98	17.6	4.89
12.3	4.26	15.9	6.22
18.2	4.38	16.1	6.58
23.9	4.50	16.4	6.38
29.3	4.62	15.7	7.43

SOURCE: Reference 1

using a gas gun. The particle impact facility is represented schematically in Figure 1, which shows in particular the arrangement used for velocity measurements.

Three light pipes connected to a light source, and three photomultipliers are positioned at fixed intervals along the particle path. The light from each pipe is intersected by the flying particle and reflected into the corresponding photomultiplier, thus inducing an electrical pulse. The pulse from the first photomultiplier triggers an oscilloscope, which then registers the pulse from the other photomultipliers. The time shift between these two pulses allows determination of the particle velocity.

The gas gun itself consists of a gas reservoir serving as a pressure source, a solenoid valve for releasing the pressure into the gun barrel, and interchangeable barrels of various inside diameter.

The small size of the specimens made it necessary to position the specimens as close as possible to the gun muzzle so as to achieve proper aiming. The distance between muzzle and specimen surface was between 1 and 5 inches for all the tests, and this limited space did not accommodate the photomultiplier array for simultaneous velocity measurement. Therefore, the impact tests were performed at predetermined pressures, without measuring the velocity. A pressure-velocity calibration curve was established separately after the tests. The pressure versus velocity curve is shown in Figure 2. Repeated velocity measurements at a given pressure indicate that the reproducibility is better than $\pm$ 2 m/s. All samples were placed on a 4-mm-thick alumina plate and mounted in an epoxy matrix. This arrangement provided a flat and steady base with similar mechanical impedance.

Table 3 summarizes the impact conditions for each of the tests performed on the various specimens. The table indicates specimen number and composition, ball size, gun pressure, and impact velocity, as well as whether the tungsten carbide ball fractured or remained intact. The latter information is of importance in evaluating the corresponding target damage. With a few exceptions, only one impact was performed for each set of conditions.

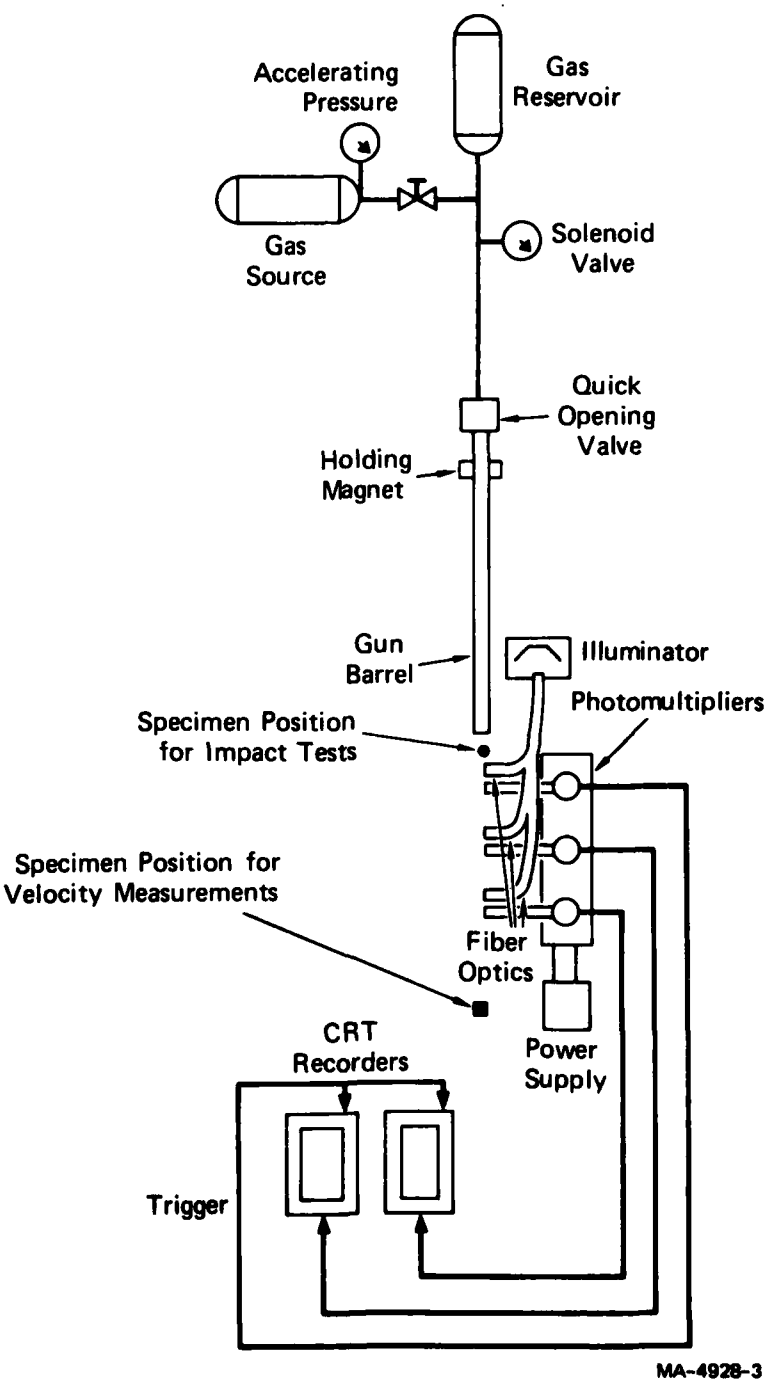

FIGURE 1 PARTICLE IMPACT TEST STAND WITH ARRANGEMENT FOR PARTICLE VELOCITY MEASUREMENTS

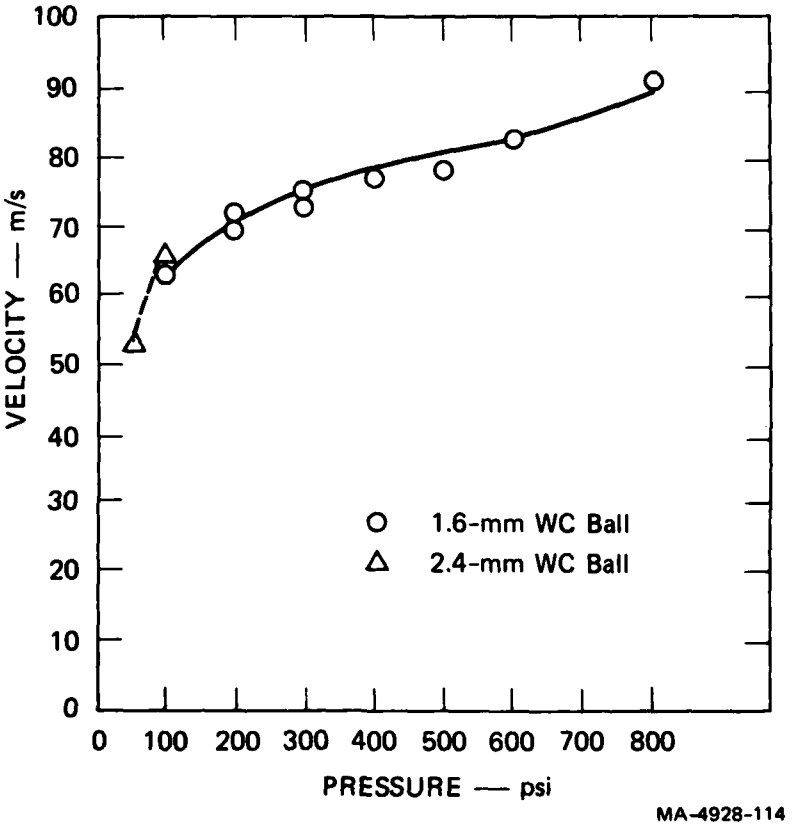

FIGURE 2 CALIBRATION OF ACCELERATING PRESSURE VERSUS BALL VELOCITY FOR THE TWO BALL SIZES USED IN THIS INVESTIGATION

Table 3.

SUMMARY OF TEST CONDITIONS

Specimen No. & Composition	TEST CONDITIONS											
	2.4-mm-Dia. WC Ball		1.6-mm-Dia. WC Ball									
	50 psi 53 m/s	100 psi 85 m/s	100 psi 83 m/s	150 psi 87 m/s	200 psi 71 m/s	250 psi 73 m/s	300 psi 74 m/s	350 psi 76 m/s	400 psi 77 m/s	500 psi 78 m/s	600 psi 82 m/s	800 psi 91 m/s
HOT PRESSED												
993 12.3 vol% ZrO_2 2.0 mol% Y_2O_3	Ball Intact	Ball Intact	--	--	--	--	--	--	--	--	--	Ball Frac
994 18.0 vol% ZrO_2 2.0 mol% Y_2O_3	Ball Intact	Ball Intact	--	--	--	--	--	--	--	--	--	Ball Frac.
995 23.9 vol% ZrO_2 2.0 mol% Y_2O_3	Ball Intact	Ball Intact	--	--	--	--	--	--	--	--	--	Ball Frac.
996 Annealed 29.3 vol% ZrO_2 2.0 mol% Y_2O_3	Ball Intact	Ball Intact	--	--	--	--	--	--	--	--	--	Ball Intact
997 29.3 vol% ZrO_2 2.0 mol% Y_2O_3	--	Ball Intact	--	--	--	--	--	--	--	--	--	Ball Frac.
SINTERED												
113 30.0 vol% ZrO_2 8.5 mol% Y_2O_3	--	Ball Intact	Ball Intact	Ball Intact	Ball Intact	Ball Intact	Ball Intact	Ball Intact	Ball Intact	--	Ball Intact	Ball Intact
114 30.0 vol% ZrO_2 1.0 mol% Y_2O_3	--	Ball Intact	Ball Intact	Ball Intact	Ball Intact	Ball Intact	Ball Intact	Ball Intact	Ball Intact	Ball Intact	Ball Intact	Ball Intact
115 30.0 vol% ZrO_2 1.5 mol% Y_2O_3	--	Ball Intact	Ball Intact	Ball Intact	Ball Intact	Ball Intact	Ball Intact	Ball Intact	Ball Intact	Ball Intact	Ball Intact	Ball Frac.
116 30.0 vol% ZrO_2 2.0 mol% Y_2O_3	--	Ball Intact	Ball Intact	Ball Intact	Ball Intact	Ball Intact	Ball Intact	Ball Intact	Ball Intact	Ball Frac.	Ball Frac.	Ball Frac.
117 Annealed 30.0 vol% ZrO_2 2.0 mol% Y_2O_3	--	Ball Frac.	Ball Frac.	--	Ball Frac.	--	Ball Frac.	--	Ball Frac.	--	--	--

Posttest Examination of the Specimens

After the tests, each impact site was examined with an optical microscope to establish the morphology and extent of damage. Because cracks are difficult to observe in Al_2O_3-based composite ceramics, we decorated the cracks by lightly polishing them on a soft cloth impregnated with a slurry of fine steel particles (~1 μm) and kerosene. However, because the crack faces were often tightly closed at the very tip, the complete crack length could not always be revealed by decorating. Therefore, the photographic records of the decorated impact surface were always double-checked with direct metallographic observations using polarized light and the minimum diaphragm aperture to detect and account for possible differences between real crack length and crack length measured on the photographs. In this study, the crack length was taken as the effectively observed length, from the rim of the permanent impression to the arrested crack tip. The metallographic observations were used to quantify the damage and establish crack size distribution curves.

Further, the diameter and depth of the permanent impression at various impact sites were measured for several specimens. Finally, the subsurface damage in selected specimens was revealed by sectioning or by removing successive layers of the impact surface. Again, subsurface crack size distributions were measured with the specific aim of assessing the effect of compressive surface residual stresses.

V RESULTS

Sintered Composite Series

Permanent Impression Depth and Diameter

The permanent impression profile was measured for selected impact sites in the five sintered specimens and the results are given in Table 4. These data should be read bearing in mind the information of Table 3 regarding the behavior of the projectile. Fracturing of the WC ball will limit the force transmitted by the projectile to the target and thus reduce the impression depth and diameter. This is particularly important for the specimens with 2.0 mol% Y_2O_3 in the as-ground and the annealed condition.

The measured profiles of the permanent impression are wide and shallow, and do not conform to a simple ball impression model (Figure 3). This is not surprising if one considers that the WC ball undergoes a slight flattening during impact.

Note from Table 4 that the impression depth is much more sensitive to compositional changes than the impression diameter. In view of this trend and recalling the fundamental definition of hardness as the resistance to penetration by an indenter, the permanent impression depth can be regarded as a measure of the hardness of the material under impact conditions. To allow an easier comparison among the five sintered specimens, the impression depth has been plotted in Figure 4 as a function of the impact velocity. It is seen that the hardness decreases with decreasing Y_2O_3 and hence tetragonal ZrO_2 content. Also, the impression depth reaches a sort of plateau for the specimen with 2.0 mol% Y_2O_3 because the WC balls start breaking above a certain velocity. The meaning of the data for the annealed specimen is less clear because in each test the ball fractured upon impact.

Table 4.
IMPRESSION DIAMETER AND DEPTH FOR IMPACTS ON THE SINTERED SPECIMENS

Impact Velocity*	Specimen 113 0.5 mol% Y_2O_3		Specimen 114 1.0 mol% Y_2O_3		Specimen 115 1.5 mol% Y_2O_3		Specimen 116 2.0 mol% Y_2O_3		Specimen 117 2.0 mol% Y_2O_3 annealed	
	Diameter D (mm)	Depth d (μm)	Diameter D (mm)	Depth d (μm)	Diameter D (mm)	Depth d (μm)	Diameter D (mm)	Depth d (μm)	Diameter D (mm)	Depth d (μm)
63	0.38	13.9	0.37	13.2	0.33	7.5	0.32	5.4	0.48 0.55	10.0 10.2
67	0.42	20.7	--	--	--	--	0.36	9.7	--	--
71	0.48	24.5	0.44	23.9	0.38	12.8	0.37	11.0	0.52	12.0
73	0.43	28.3	--	--	--	--	0.37	12.8	--	--
74	0.50	32.4	0.51	30.6	0.58	12.8	0.46	14.5	0.56	16.4
76	0.52	35.8	--	--	--	--	0.43	11.8	--	--
77	0.51	34.0	0.53	30.1	0.53	23.2	0.44	10.4	0.58	14.5
78	--	--	0.51	33.4	0.47	25.2	0.48	11.1	--	--
82	--	--	0.53	35.2	0.51	27.8	0.49	10.0	--	--
91	0.55	42.0	0.56	38.2	0.50	29.1	0.48	14.3	--	--

*1.6-mm-diameter WC Ball

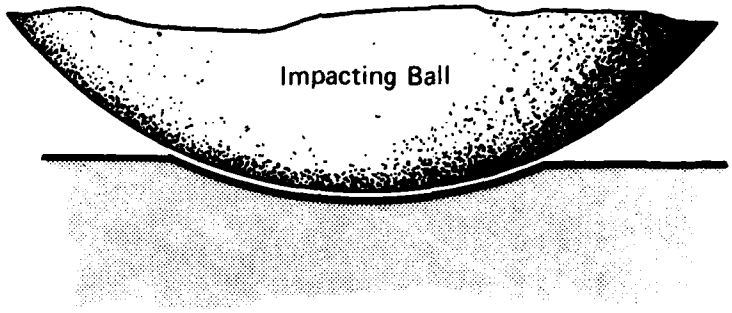

(a) SIMPLE IMPRESSION MODEL

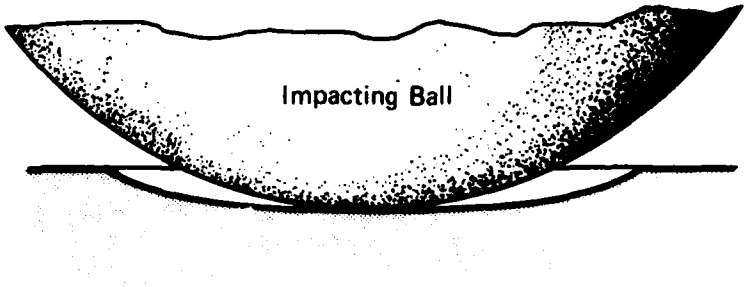

(b) IMPRESSION OBSERVED EXPERIMENTALLY

MA-4928-115

FIGURE 3 PERMANENT IMPRESSION (a) RESULTING IN THE CASE OF SIMPLE BALL IMPRESSION MODEL (b) OBSERVED EXPERIMENTALLY

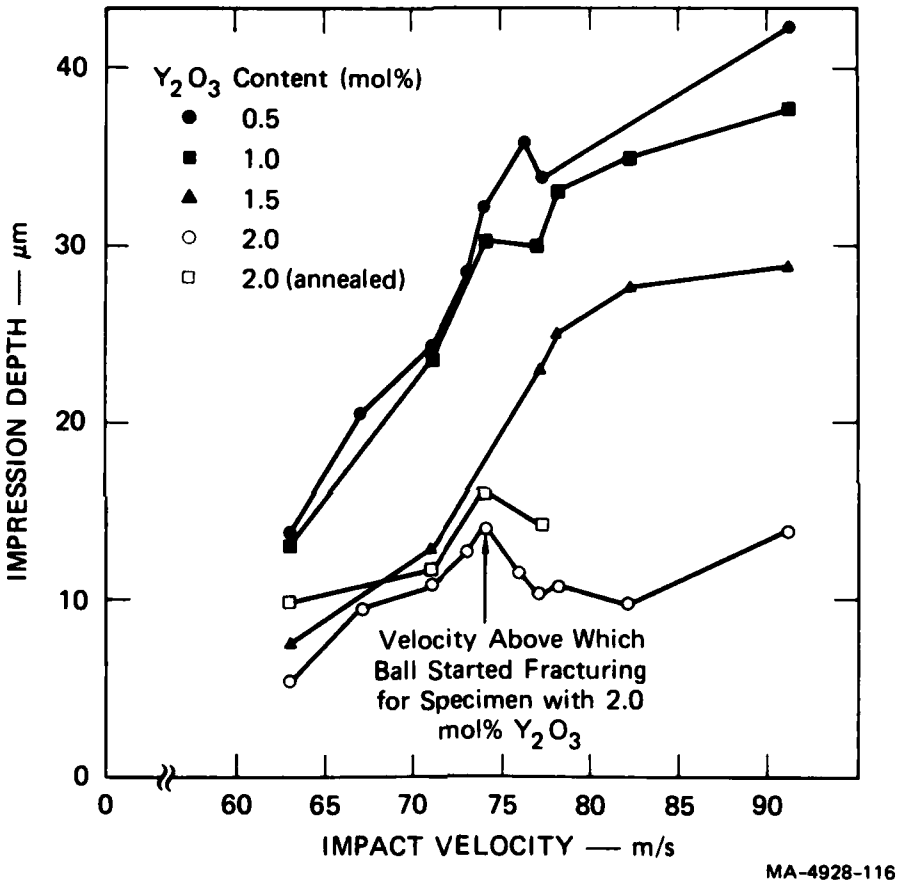

FIGURE 4 PERMANENT IMPRESSION DEPTH AS A FUNCTION OF IMPACT VELOCITY FOR SINTERED SPECIMENS

Damage Morphology

The dominant failure mechanism for specimens of the sintered composite series was radial cracking, although limited and shallow ring cracking was also observed. The ring cracks were confined to the very edge and the interior of the permanent impression. Figures 5 to 7 show micrographs of impact sites in the different materials produced under various impact conditions. Note that in all the micrographs the cracks have been decorated before observation, Figures 5, 6, and 7 illustrate the evolution of damage with increasing impact velocity of a 1.6-mm WC ball in specimens containing 0.5 mol% Y_2O_3 in the as-ground condition and 2.0 mol% Y_2O_3 in the as-ground and in the annealed condition. It is seen that in the as-ground specimens, the damage is very sensitive to impact velocity. As indicated in Table 3, the projectile ball fractured upon impact with the annealed specimen for all the test conditions investigated. This explains the lack of marked differences in cracking for the cases of Figure 7, because the damage to the target is limited by the strength of the projectile.

A comparison of the damage in the five sintered specimens resulting from identical test conditions is given in Figure 8. Here again, the WC ball fractured upon impacting the annealed specimen.

The extent of the radial cracks below the surface is revealed in the cross sections of Figure 9 and Figure 10 for specimens with 0.5 and 2.0 mol% Y_2O_3, respectively. The depth of the cracks is about the same for similar test conditions. The surface ring cracks are hardly seen in the cross sections. In Figure 10 it is worth noting that the left radial crack that propagated below the surface to link up with the crack at the center has grown as a result of the sectioning operation. This can be seen by comparing Figure 6 and Figure 10, which represent the same impact site before and after sectioning. The subsurface linkup of the crack as well as the crack propagation upon sectioning have been observed at other locations in this specimen.

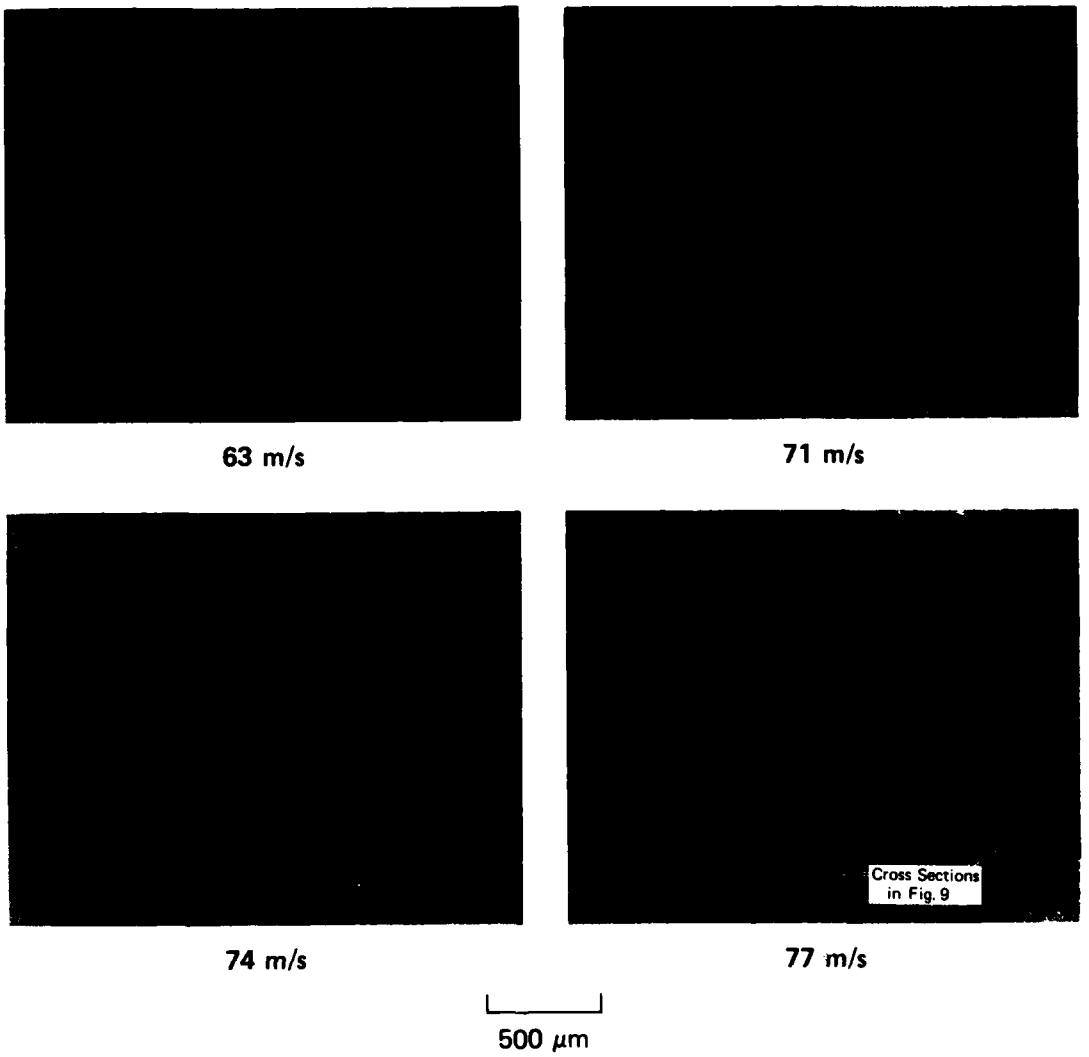

FIGURE 5 DAMAGE PRODUCED IN SINTERED SPECIMEN WITH 0.5 mol% Y_2O_3 BY 1.6-mm WC BALL IMPACTING AT SEVERAL VELOCITIES

(Polarized light micrographs)

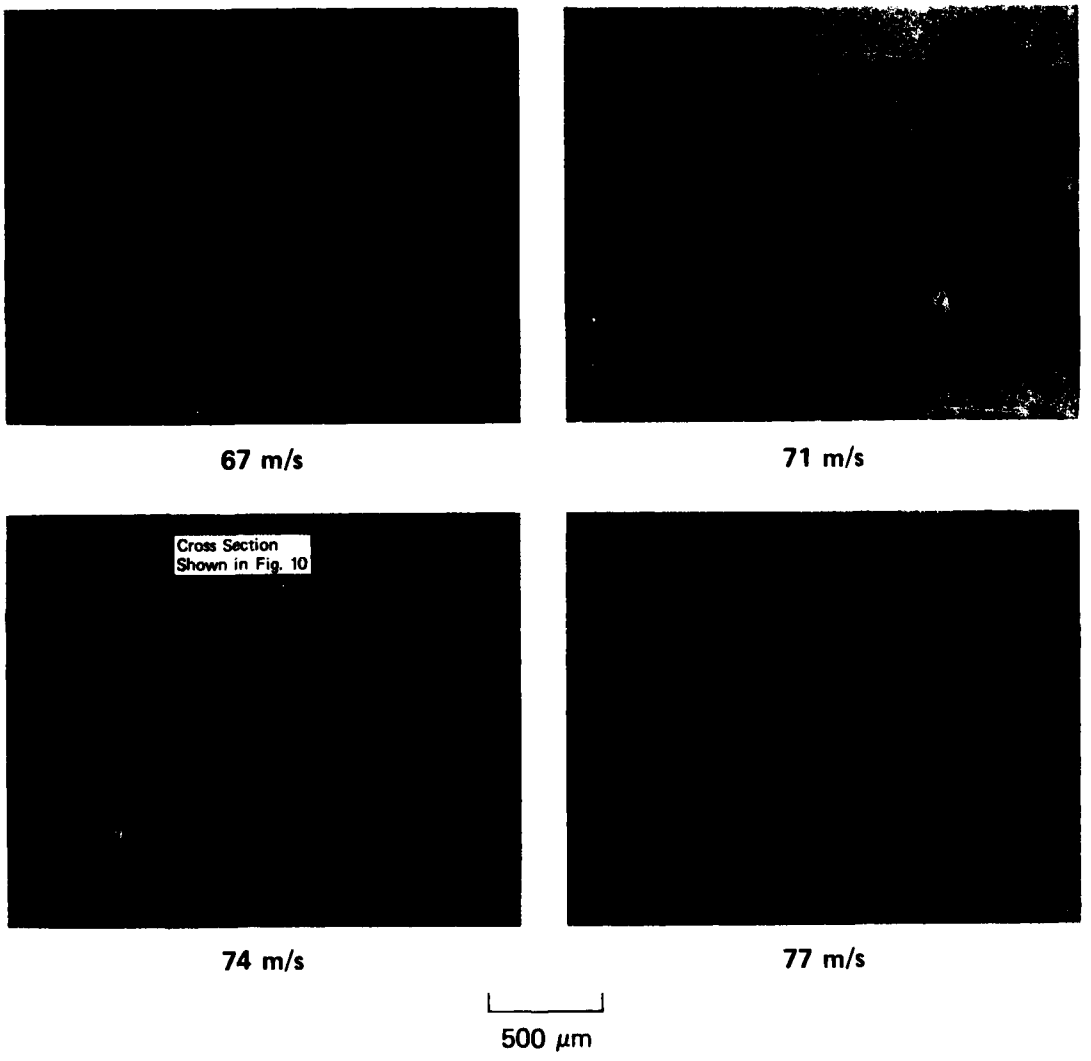

FIGURE 6 DAMAGE PRODUCED IN SINTERED SPECIMEN WITH 2.0 mol% Y_2O_3 BY 1.6-mm WC BALL IMPACTING AT SEVERAL VELOCITIES

(Polarized light micrographs)

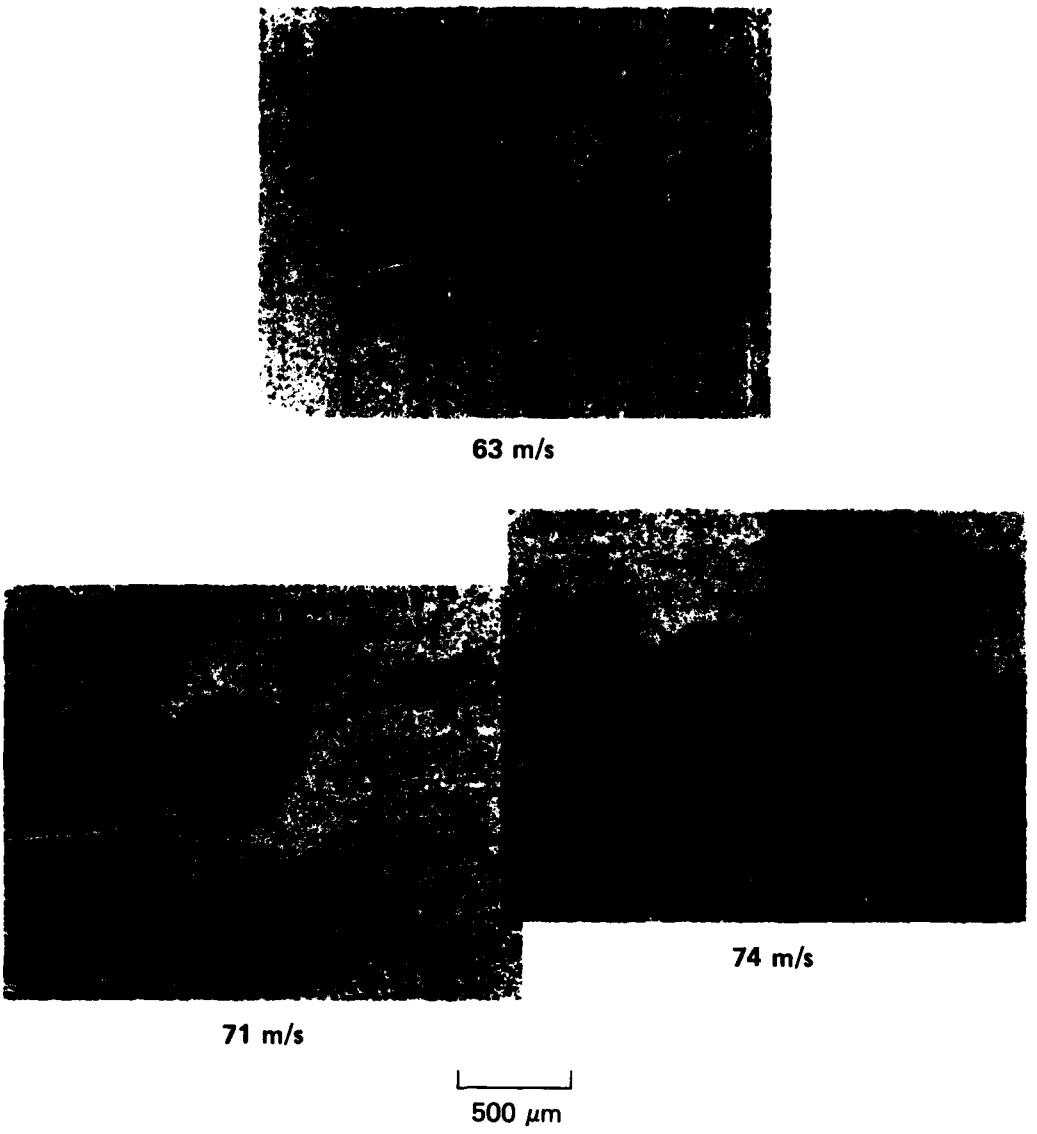

FIGURE 7 DAMAGE PRODUCED IN SINTERED SPECIMEN WITH 2.0 mol% Y_2O_3 (Annealed) BY 1.6-mm WC BALL IMPACTING AT SEVERAL VELOCITIES. NOTE CRACK INTERACTION.

(Bright light micrographs)

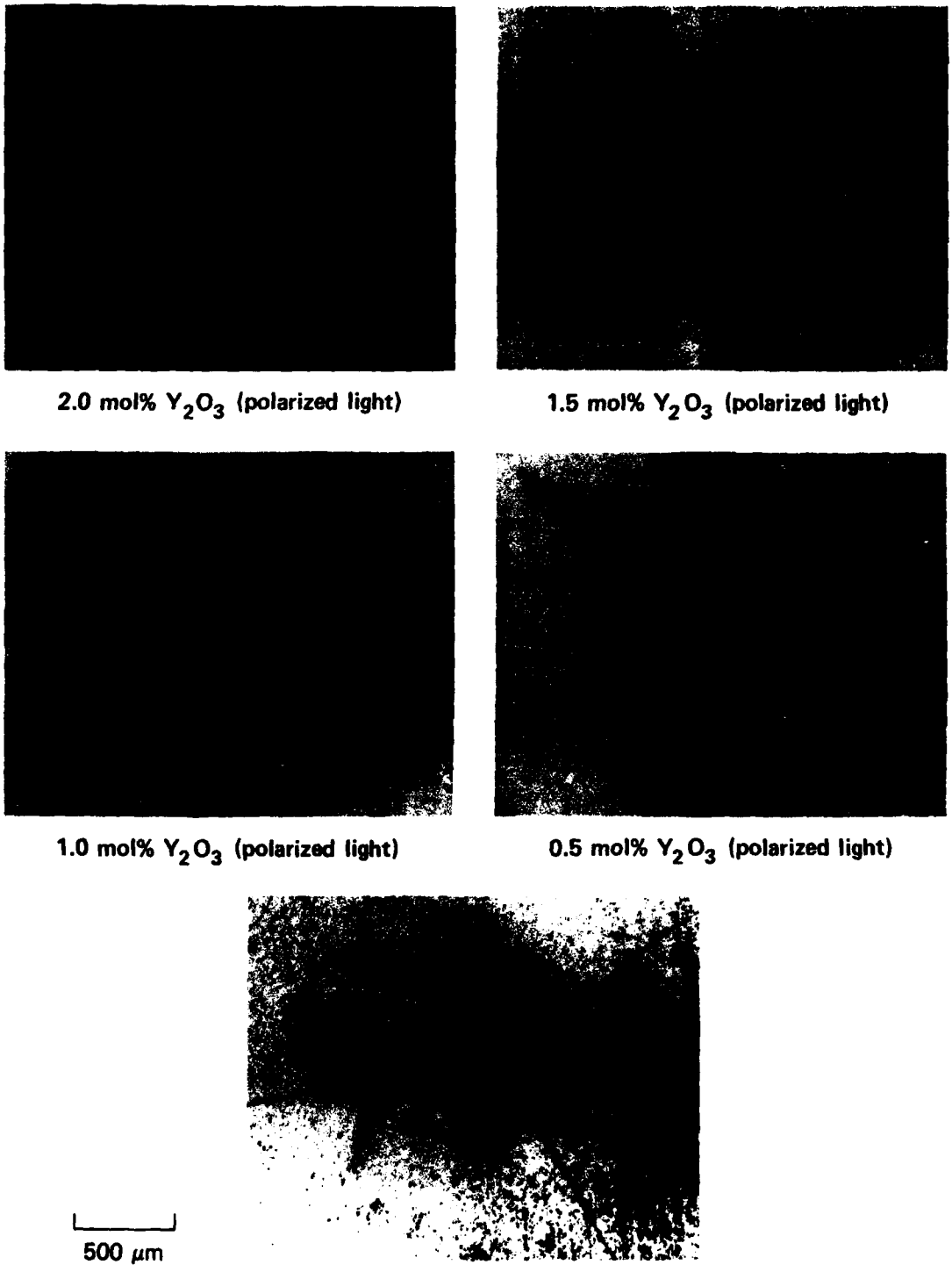

FIGURE 8 COMPARISON OF IMPACT DAMAGE IN SINTERED SPECIMENS OF VARYING Y_2O_3 CONTENT CAUSED BY IMPACT OF A 2.4-mm WC BALL AT A VELOCITY OF 65 m/s

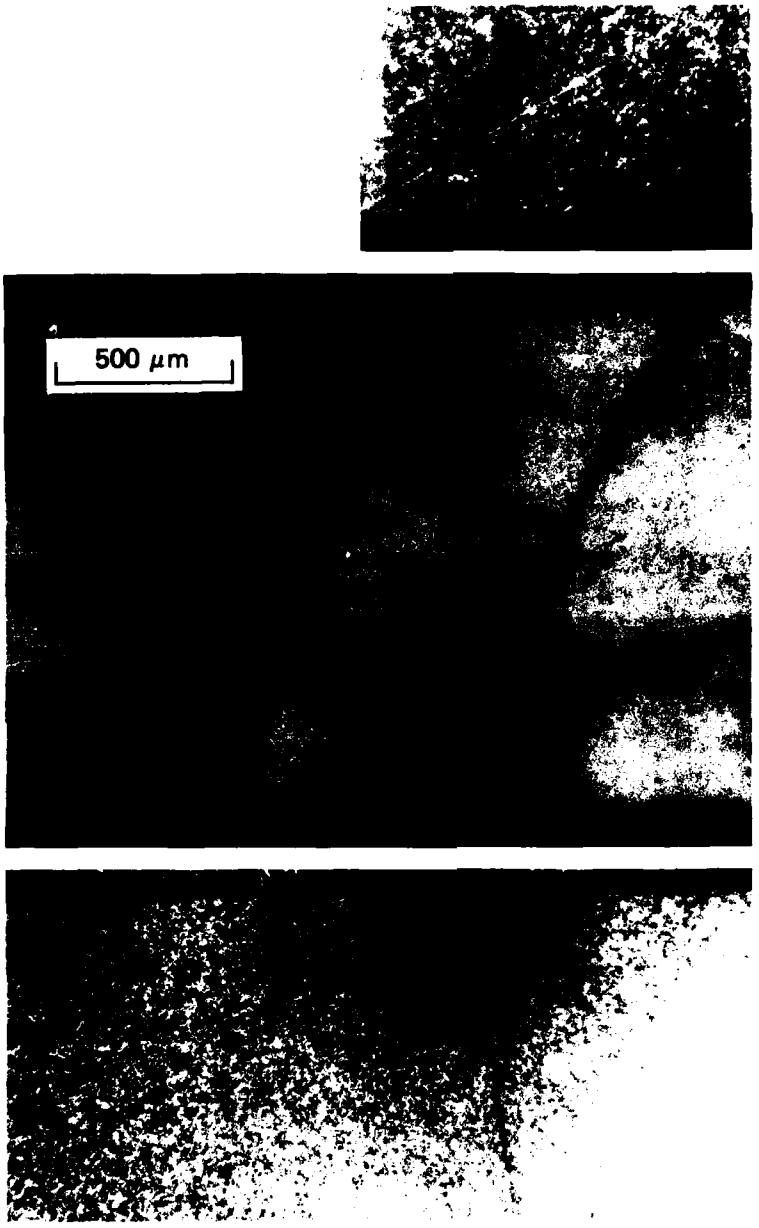

FIGURE 9 SUBSURFACE DAMAGE IN SINTERED SPECIMEN WITH 0.5 mol% Y_2O_3 CAUSED BY IMPACT OF A 1.6-mm WC BALL AT A VELOCITY OF 77 m/s

FIGURE 10 SUBSURFACE DAMAGE IN SINTERED SPECIMEN WITH 2.0 mol% Y_2O_3 CAUSED BY IMPACT OF A 1.6-mm WC BALL AT A VELOCITY OF 74 m/s

Crack Size Distribution in the Impact Surface

The crack size distributions for the sintered composite series were determined from photographs of the impact sites in which the apparent crack lengths had been corrected to reflect the actual crack length as observed using the special illumination technique described in Section IV.

Crack size distributions in specimens with 0.5 and 2.0 mol% Y_2O_3 are given in Figure 11 for 1.6-mm WC balls at increasing impact velocities. These plots indicate how damage develops under progressively more severe impact conditions. Although some overlapping occurs at higher velocities, the plots show a definite shift towards more cracks and larger cracks as the velocity becomes higher. Comparison of the crack size distributions in Figure 11a and 11b indicate that the damage measured on the impact surface is greatly reduced for the specimen with higher Y_2O_3 and hence tetragonal ZrO_2 content. A further comparison between the various compositions is given in Figure 12, which shows crack size distributions in the five sintered specimens for three sets of impact conditions. In addition, the crack size distribution 25 μm below the impact surface is also plotted for the specimen with 1.5 mol% Y_2O_3 (see discussion below). Figure 12 indicates that specimens having a higher Y_2O_3 content (1.5 and 2.0 mol%), and hence a larger amount of tetragonal ZrO_2, experience significantly reduced damage in the impact surface. However, the specimen with 2.0 mol% Y_2O_3 in the annealed condition displays much more extensive cracking than the specimen with the same composition but in the as-ground condition. The damage is comparable to, or greater than, the damage in specimens with 0.5 and 1.0 mol% Y_2O_3.

Because the ring cracks were shallow and located mainly within the permanent impression so that they could not be observed easily, a quantification of the ring crack damage was not attempted.

Crack Size Distribution Below the Impact Surface

Successive layers were ground off the specimen with 1.5 mol% Y_2O_3 and the crack size distribution below the impact surface was established for depths of approximately 5 μm and 25 μm. It was found that the crack size distributions at 5 μm and 25 μm were identical but differed markedly

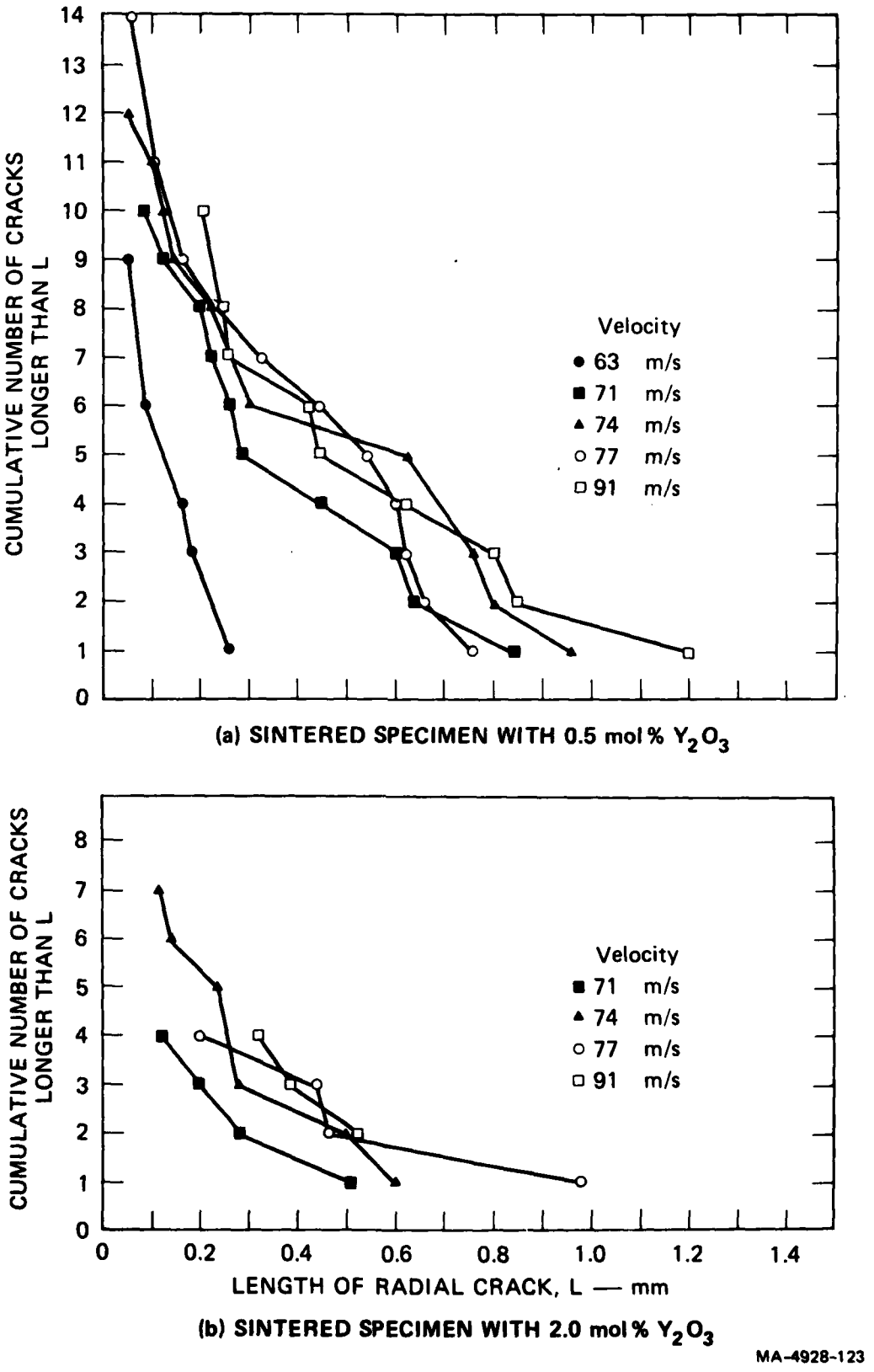

FIGURE 11 SIZE DISTRIBUTIONS OF RADIAL CRACKS FOR TWO SINTERED SPECIMENS OF DIFFERENT Y_2O_3 CONTENT AND IMPACTED AT VARIOUS VELOCITIES

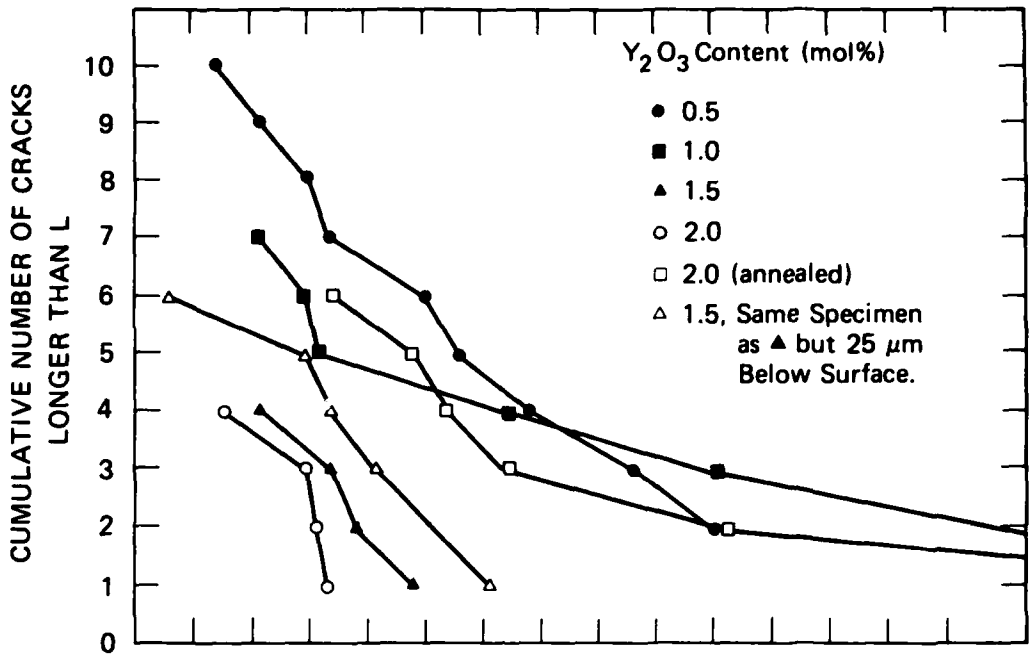

(a) 2.4-mm WC BALL, 65 m/s

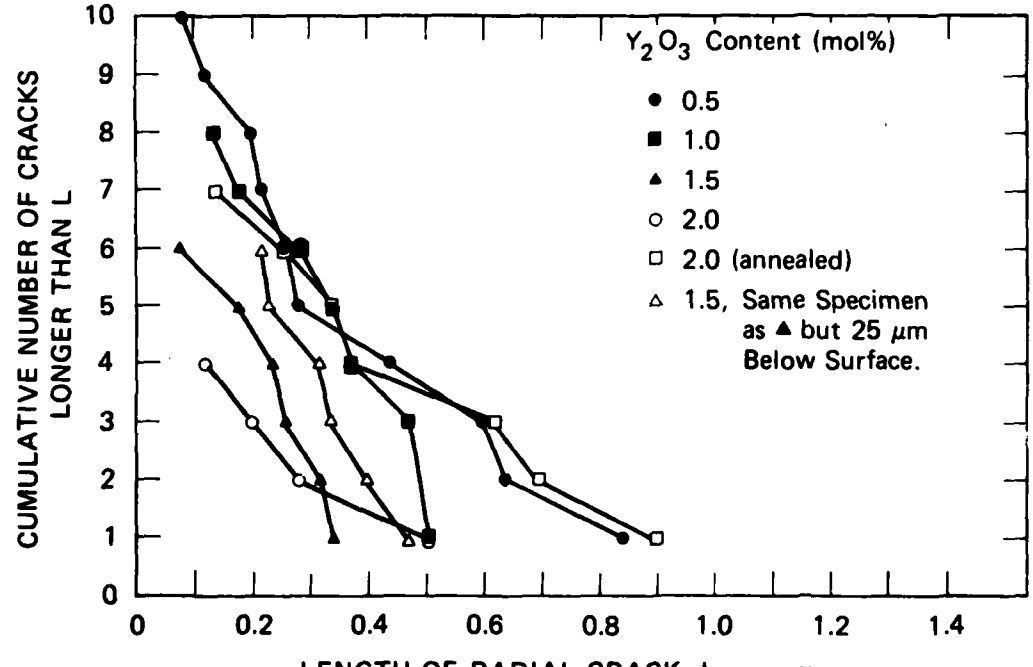

(b) 1.6-mm WC BALL, 71 m/s

MA-4928-124

FIGURE 12 COMPARISON OF SIZE DISTRIBUTIONS OF RADIAL CRACKS FOR SINTERED SPECIMENS OF VARYING COMPOSITION AT THREE TEST CONDITIONS

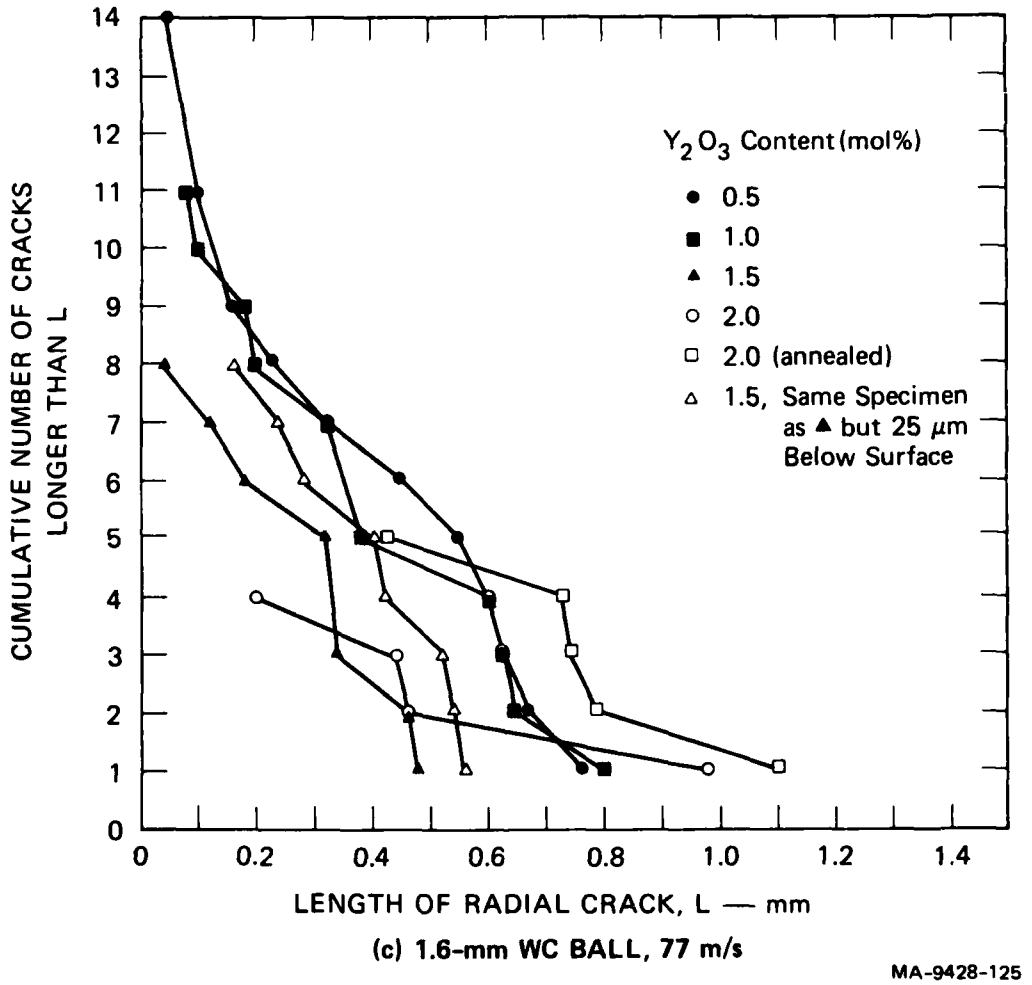

FIGURE 12 COMPARISON OF SIZE DISTRIBUTIONS OF RADIAL CRACKS FOR SINTERED SPECIMENS OF VARYING COMPOSITION AT THREE TEST CONDITIONS (Concluded)

from the crack size distribution in the impact plane. This observation is illustrated in Figure 12 where both the surface data and the data at a 25-μm depth are compared for three sets of impact parameters. For given test conditions, the distributions are almost identical in shape, but the curve representing the subsurface damage is displaced to the right.

A similar grinding procedure was used to assess the subsurface damage in the specimen with 0.5 mol% Y_2O_3. Removal by grinding of a 10-μm layer revealed no change in the crack size distribution observed on the impact surface. Thus, we concluded that the specimen composition affects the shape of the radial cracks in the plane of extension perpendicular to the impact surface, as illustrated in Figure 13. In the specimen containing an appreciable amount of ZrO_2, the cracks do not fully extend to the surface and a small ligament remains unbroken. The retarded growth near the surface can be explained by the presence of compressive residual stresses, which tend to reduce the amplitude of the tensile stresses arising during impact. The grinding away of a surface layer could have various effects. It could remove a layer containing the unbroken ligament and reveal the full extent of the cracks, or alternatively, it could induce the rupture of the unbroken ligament either by direct mechanical action or by perturbing the stress equilibrium by removal of material. The results obtained on the specimen with 0.5 mol% Y_2O_3 demonstrate that under normal conditions, when the radial cracks have propagated completely to the surface, grinding does not cause any further crack extension.

These crack shape differences suggest that the impact damage in specimens with a higher tetragonal ZrO_2 content should be assessed on the basis of subsurface observations rather than observations of the impact surface. If this is done for the specimen with 1.5 mol% Y_2O_3 using the data in Figure 12, the impact damage is still reduced, though to a lesser extent, when compared with specimens containing 0.5 and 1.0 mol% Y_2O_3 or with the annealed specimen.

The difference in surface and subsurface crack size distributions in the specimen with 1.5 mol% Y_2O_3 as well as the poor impact resistance

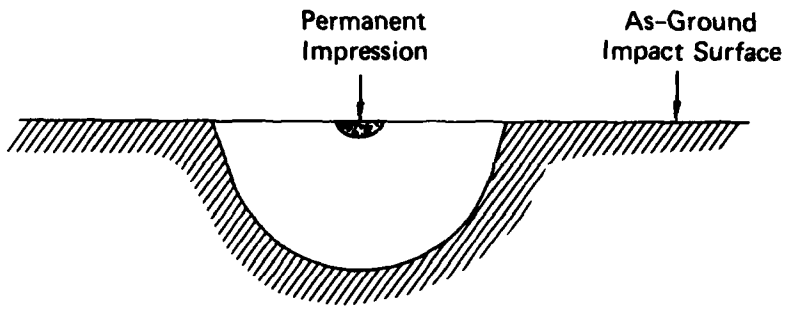

(a) SPECIMENS WITH NO TETRAGONAL ZrO_2

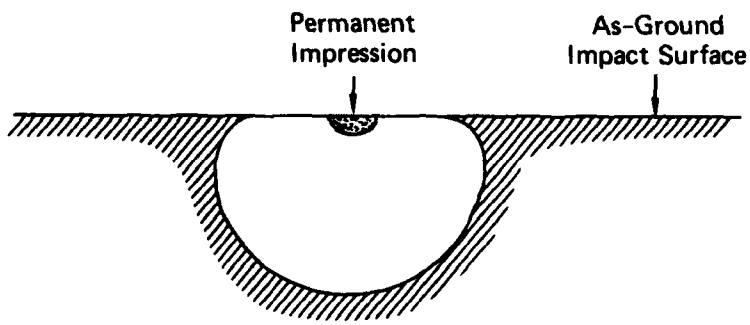

(b) SPECIMENS WITH APPRECIABLE AMOUNTS OF TETRAGONAL ZrO_2

MA-4928-126

FIGURE 13 SCHEMATIC REPRESENTATION OF THE SHAPE OF AN EXTENDED RADIAL CRACK IN SPECIMENS WITH DIFFERENT AMOUNTS OF TETRAGONAL ZrO_2

of the annealed specimen with 2 mol% Y_2O_3 strongly suggest that compressive surface residual stresses play an essential role in improving the impact resistance of the composite ceramics.

Hot-Pressed Composite Series

Permanent Impression Depth and Diameter

Table 5 presents the few measurements of the permanent impression depth and diameter made on specimens with 12,3 and 29.3 vol% ZrO_2 in the as-ground condition and on the specimen with 29.3 vol% in the annealed condition. Two values are given when two impact tests were performed for the same conditions on the same specimen to indicate the reproducibility of the measurements.

Table 5 shows that the dynamic hardness of the hot-pressed composites decreased as the volume fraction of ZrO_2 increased. This observation is consistent with the static hardness data of Table 2. Moreover, annealing further softens the specimen. Comparison of the impression depth data for the sintered and hot-pressed series indicates that the hot-pressed materials are harder. This is not surprising if one considers that hot-pressed materials are likely to be denser than sintered materials.

As for the sintered composite series the impression profiles for the hot-pressed series are wide and very shallow (Fig. 3b). The impression depth seems also to be much more sensitive to compositional changes than the impression diameter.

Damage Morphology

As was the case in the sintered composite series, the impact damage in the hot-pressed composite series is predominantly radial cracking with some shallow ring cracking. Figures 14 to 17 show selected impact sites for different specimens, as well as some cross sections. Here again, in all the photographs, the cracks were decorated before observation. From Figure 14c and Figure 15c it is seen that the ring cracks, when they are observed, are very shallow and never reach a significant depth. The radial cracks, however, have an appreciable depth (0.5 to 1.0 mm or more)

Table 5.

IMPRESSION DIAMETER AND DEPTH FOR SELECTED IMPACT CONDITIONS IN THREE HOT-PRESSED SPECIMENS

IMPACT CONDITIONS	SPECIMEN 993 12.3 vol% ZrO_2		SPECIMEN 996 29.3 vol% ZrO_2 Annealed		SPECIMEN 997 29.3 vol% ZrO_2	
	Diameter D (mm)	Depth d (μm)	Diameter D (mm)	Depth d (μm)	Diameter D (mm)	Depth d (μm)
2.4-mm WC ball 53 m/s	0.44-0.52	1.8-2.5	--	--	0.54	3.7
2.4-mm WC ball 65 m/s	0.56-0.66	3.6-3.8	0.56	11.0	0.60-0.68	5.1-6.2
1.6-mm WC ball 91 m/s	--	--	0.49	21.0	0.64	7.1*

*Ball fractured upon impact.

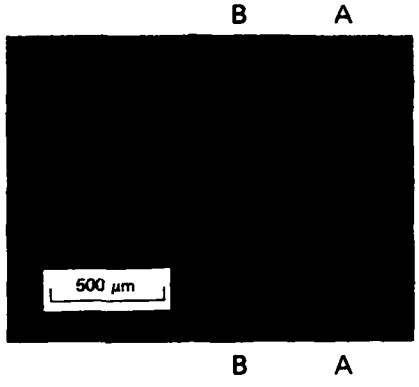

(a) IMPACT DAMAGE ON SURFACE OF SPECIMEN

Note the ring cracks and two radial cracks.

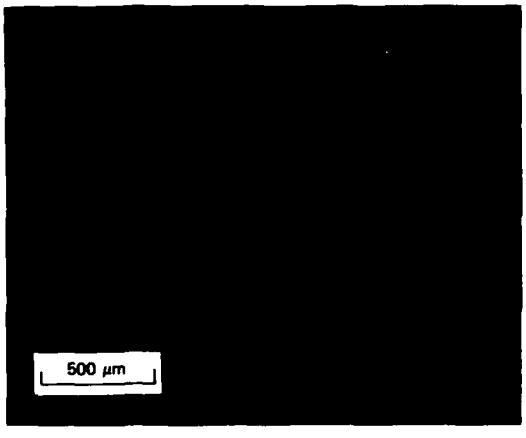

(b) CROSS SECTION A-A IN FIGURE 14(a), SHOWING DEPTH OF RADIAL CRACK

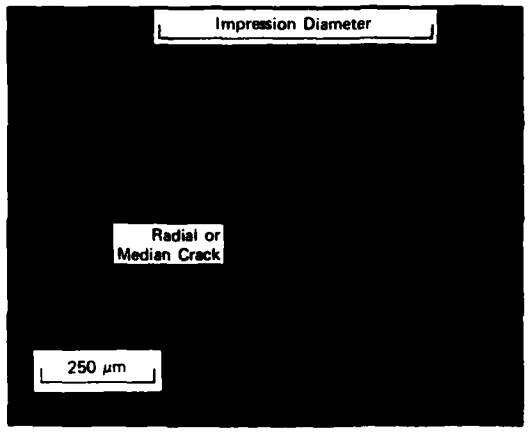

(c) CROSS SECTION B-B IN FIGURE 14(a), SHOWING SUBSURFACE DAMAGE WITHIN THE IMPRESSION DIAMETER AND RADIAL OR MEDIAN CRACK

MP-4928-127

FIGURE 14 IMPACT DAMAGE IN HOT-PRESSED SPECIMEN WITH 12.3 vol% ZrO_2 CAUSED BY IMPACT OF A 2.4-mm WC BALL AT A VELOCITY OF 65 m/s

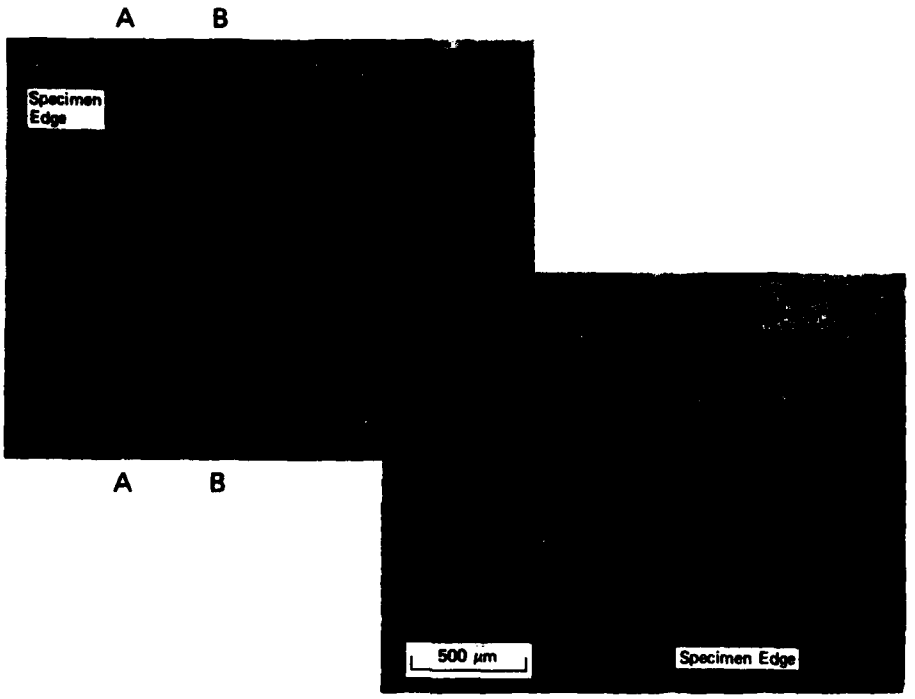

(a) IMPACT DAMAGE ON SURFACE OF SPECIMEN

Test conditions: upper left impact site, 1.6-mm WC ball, velocity of 91 m/s; lower right impact site, 2.4-mm WC ball, velocity of 65 m/s. Note the absence of ring cracks, the interaction of radial cracks from adjacent impact sites, and the influence of the specimen boundary on cracking.

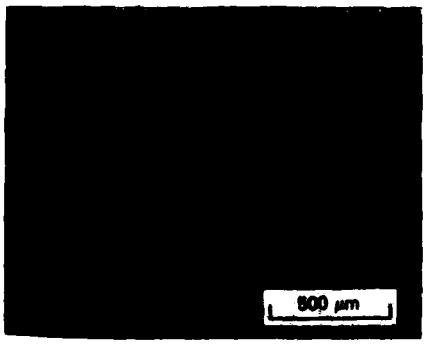

(b) CROSS SECTION A-A IN FIGURE 15(a), SHOWING SUBSURFACE EXTENT OF RADIAL CRACKS

Note that the crack on the right in Figure 15(a) has extended all the way underneath the impact impression and appears as the median crack in the cross section.

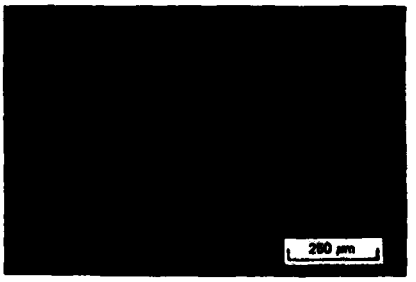

(c) CROSS SECTION B-B IN FIGURE 15(a), SHOWING SUBSURFACE DAMAGE WITHIN THE IMPRESSION DIAMETER AND RADIAL OR MEDIAN CRACK

MP-4928-128

FIGURE 15 IMPACT DAMAGE IN HOT-PRESSED SPECIMEN WITH 29.3 vol% ZrO_2

MP-4928-129

FIGURE 16 IMPACT DAMAGE IN HOT-PRESSED SPECIMEN WITH 29.3 vol% ZrO_2 IN THE ANNEALED CONDITION

Test conditions: 1.6-mm WC ball, velocity 91 m/s.

MP-4928-130

FIGURE 17 IMPACT DAMAGE IN HOT-PRESSED SPECIMEN WITH 29.3 vol% ZrO_2 IN THE ANNEALED CONDITION

Test conditions: 2.4-mm WC ball, velocity 65 m/s.

comparable to their extent in the impact surface (Figures 14b and 15b). Note also that the damage is more pronounced and better defined in the annealed specimens than in the as-ground specimens (Figures 16 and 17).

Finally, as shown in Figure 15a, crack interaction with the boundaries as well as with cracks from adjacent impact sites was often observed. This is mainly due to the small size of the specimens and makes the interpretation of the results difficult.

Crack Size Distribution

The size distribution of radial cracks for various hot-pressed specimens is presented in Figure 18 for the impact conditions 2.4-mm ball and 65 m/s velocity and 1.6-mm ball and 91 m/s velocity. In the former case Figure 18a indicates that the impact damage increases with increasing ZrO_2 content. For the latter case the WC balls fractured for all specimens except the annealed sample. This limits the usefulness of the data for evaluating the impact resistance of the various compositions, because the crack size distribution is no longer controlled by the material properties of the target, but by the strength of the projectile. Nevertheless, Figure 18b indicates that the specimen with the lowest ZrO_2 content has the best impact resistance. From both Figure 18a and 18b, it is also clear that, with a few exceptions, more cracks are nucleated in the annealed specimen than in the rest of the batch. Furthermore, the cracks in the annealed specimen tend to be longer.

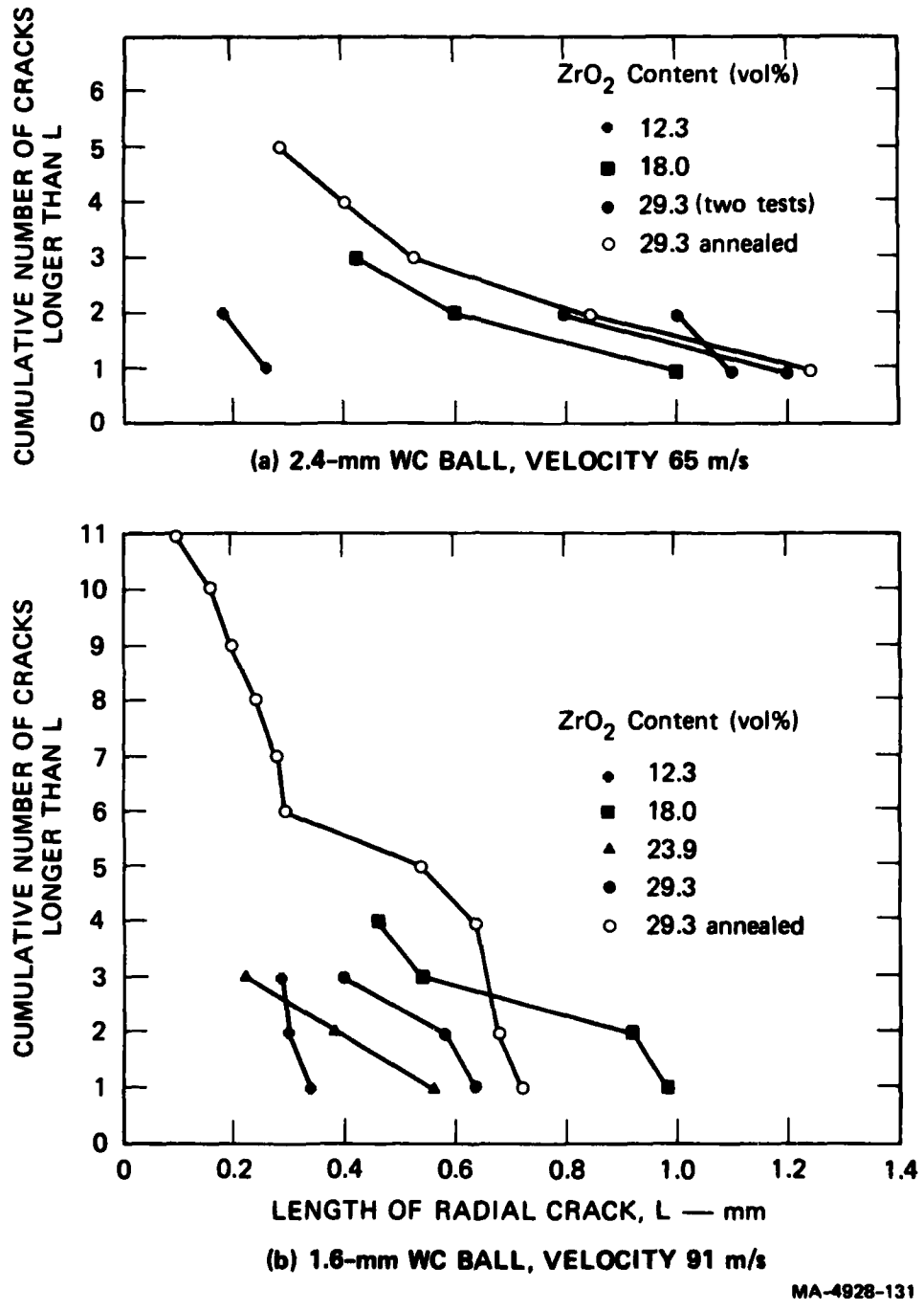

FIGURE 18 EFFECT OF ZrO_2 CONTENT ON SIZE DISTRIBUTION OF RADIAL CRACKS PRODUCED IN HOT-PRESSED Al_2O_3-ZrO_2 SPECIMENS UNDER TWO TEST CONDITIONS

VI DISCUSSION

1. Preliminary Remarks on the Mechanics of Impact Damage

Before discussing the results presented in the previous section, it is appropriate to review the various parameters that influence the cracking of a target impacted by a particle. These parameters and their interaction are represented in Figure 19.

Neglecting statistical aspects of the spatial and size distribution of inherent flaws, the morphology of the damage and its extent are controlled by the stress field resulting from the impact and the fracture toughness of the target material. The stress field itself is a complex function of the impact conditions (ball size and velocity) and the mechanical properties of both the target and the projectile materials. The relative hardness of target and projectile will determine which one of the two yields first, and this in turn determines the stress field and the cracking pattern. If the target remains elastic for all impact conditions, the maximum tensile stress is directed radially in the impact plane and ring and cone cracking is the dominant damage mode.[11,12] On the contrary, if the projectile is harder than the target, yielding will occur in the target and the hoop stress becomes tensile. Although ring cracking still occurs, radial cracking becomes the dominant mode.[11,12]

Besides the hardness, the fracture strength of the projectile also plays a decisive role in determining the impact damage. As has already been mentioned, failure of the projectile interrupts the load transfer and limits the damage to the target.

Finally, because cracking is a result of tensile stresses developing during impact, the presence of compressive residual stresses in the zones of high applied tensile stresses will also tend to reduce the damage.

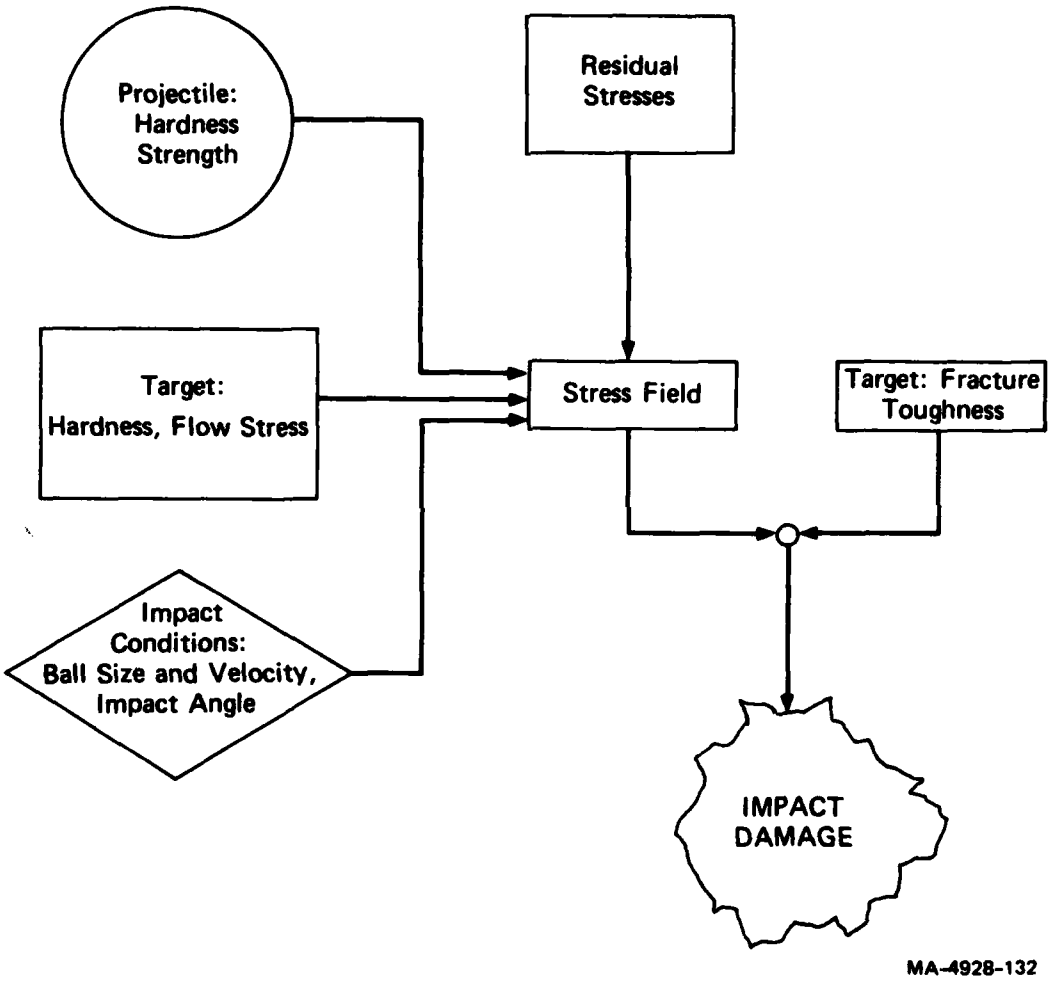

FIGURE 19 INTERACTION OF PARAMETERS INFLUENCING THE IMPACT DAMAGE

This simplified discussion of the mechanics of impact damage will be useful in assessing the results of the preceding section. Changing the chemical and phase composition of the composites may change the hardness, flow stress, and fracture toughness of the target. Grinding operations may change the surface residual stresses (Figure 19). We now turn to the question: Which of these parameters controls the observed results?

Sintered Composite Series

The results of the tests on the sintered composite series clearly showed that some improvement in the impact resistance of the $Al_2O_3 \cdot xZrO_2$ system can be obtained when the ZrO_2 is retained in the tetragonal phase. An increase in fracture toughness with the amount of tetragonal ZrO_2 cannot account for the observed gain in impact resistance, because the annealed specimen with 2.0 mol% Y_2O_3 was as damaged as the specimens with mainly monoclinic ZrO_2. Changes in hardness with composition also cannot explain the change in impact resistance for two reasons. First, the reduced hardness of specimens with 0.5 and 1.0 mol% Y_2O_3 is probably due mainly to the high density of microcracks that were observed in these composites.[10] Second, the annealed specimen appears to have about the same hardness as specimens with 1.5 and 2.0 mol% Y_2O_3 and yet displays important damage. The high microcrack density in specimens with 0.5 and 1.5 mol% Y_2O_3 may explain their poor performance, but gives no clues to why specimens with higher Y_2O_3 content in the as-ground condition showed reduced damage and the annealed specimen did not.

The only possible answer, which has already been alluded to, is that surface compressive residual stresses that are induced during grinding are responsible for the enhanced impact resistance of $Al_2O_3 \cdot xZrO_2$ composites with retained tetragonal ZrO_2. Residual stresses caused by surface oxidation have already been shown to improve significantly the impact properties of $Si_3N_4 \cdot$ 20 vol% ZrO_2 composites.[13] In the present $Al_2O_3 \cdot xZrO_2$ hot-pressed composites, residual stresses of the order of 100 ksi have been measured and the thickness of the layer affected by compressive radial stresses ranged between 7 and 30 μm.[10]

Some of the observations made during this study are evidence that residual stresses are present in the specimen with higher tetragonal ZrO_2 content. The difference in impact surface and subsurface crack size distribution in the specimen with 1.5 mol% Y_2O_3 can be explained as an effect of compressive residual stresses retarding the crack growth in the surface layer or possibly tightly closing the crack tips so that they cannot entirely be decorated and observed. Note that the thickness of the layers removed in the specimen with 1.5 mol% Y_2O_3 is of the order of the values quoted above for the thickness of the layer affected by residual stresses.

Further, the fact that some of the cracks in the specimen with 2.0 mol% Y_2O_3 extended upon sectioning can also be regarded as an effect of residual stresses. Sectioning disturbs the balance of stresses and the nonequilibrated tensile stresses relax, propagating the crack.

The data of Figures 11 and 12 suggest that both crack nucleation and crack growth are affected by the residual stresses. Although the detailed mechanisms are not yet understood, the residual stresses could improve the impact resistance in various ways. If it is assumed that radial cracks initiate at microcracks in a region slightly below the impact surface when a critical tensile stress (or stress intensity factor) is reached, then the presence of compressive residual stresses superimposed on the impact stresses will reduce the net applied stress. Hence, more severe impact conditions would be required to initiate cracking. It is also conceivable that the residual stresses would modify the development of the permanent impression and increase the apparent hardness of the material.

Additional tests are needed to establish nucleation threshold values and to clarify the mechanisms by which residual stresses improve the impact resistance.

Hot-Pressed Composite Series

Because of small specimen size, the tests on the hot-pressed composite series yielded only limited information on the impact resistance of the various materials. In many cases radial cracks propagated out to the specimen edges, and in other cases, cracks from two neighboring impact sites often interacted and joined up. Examples are given in Figure 15a. The small amount of area available for impact also precluded the performance of tests under a wider range of impact conditions.

Despite these difficulties, it is clear that the annealed material with 29.3 vol% ZrO_2 has the lowest impact resistance, that the dynamic hardness of the hot-pressed materials decreases with increasing ZrO_2 content, and that impact resistance decreases with increasing ZrO_2 content.

The poor impact resistance of the annealed material suggests that the increase in toughness associated with the 29.3 vol% tetragonal ZrO_2 composition does not warrant, per se, improvements in impact resistance. The high impact damage in the annealed specimen may also be explained by reduction processes during hot-pressing, and reoxidation during annealing, which in specimens with higher ZrO_2 content causes surface cracking and spalling and hence significant degradation of the impact resistance.[14]

The trends in the dynamic hardness and impact resistance for non-annealed specimens can be interpreted as follows: Increases in the tetragonal ZrO_2 content tend to promote the development of compressive residual stresses in the surface layer upon grinding. The results obtained in the sintered materials show that this is a beneficial effect. On the other hand, increases in ZrO_2 content lower the dynamic hardness so that a deeper permanent impression and very likely higher circumferential tensile stresses result. This, in turn, favors the nucleation of radial cracks. Thus the impact resistance of the composite material containing tetragonal ZrO_2 would be determined by a balance of these two opposing effects and there should be an optimum ZrO_2 content beyond which no more improvements would be obtained. From our results we deduce that this optimum value of the ZrO_2 content should be 12 vol% or smaller. On the other hand, cracking caused by the reduction process during hot-

pressing may well play a role in decreasing the impact resistance of materials with more than 12 vol% ZrO_2. Additional experiments on larger specimens are needed to establish clear trends and to verify these ideas.

VII CONCLUSIONS

The morphology of the damage in hot-pressed and sintered $A\ell_2O_3 \cdot xZrO_2$ specimens of various chemical and phase compositions caused by impact with WC balls is predominantly radial cracking. Some shallow ring cracks also form, but their contributions to the damage is negligible.

Damage in the sintered composite series (as measured by the radial crack size distribution in the impact plane) decreased markedly with increasing tetragonal ZrO_2 content, indicating that the retention of tetragonal zirconia enhances the impact resistance of $Al_2O_3 \cdot xZrO_2$ composite ceramics. Annealing reduced the impact resistance to that of the monoclinic material, suggesting that the enhancement results from surface compressive residual stresses induced by grinding.

In the hot-pressed specimens where only limited information was obtained, observed decreases in dynamic hardness and increases in impact damage with increasing ZrO_2 content suggest that in composites where the total ZrO_2 content varies, the impact resistance is determined by the balance of the beneficial effect of surface residual stresses and the detrimental decrease in hardness.

REFERENCES

1. F. F. Lange, "Transformation Toughening in the Al_2O_3/ZrO_2 Composite System," ONR Rept. No. 7, Contract N00014-77-C-0441 (October 1979).
2. R. N. Pratil and E. C. Subbarao, J. Appl. Cryst. 2, 281 (1969).
3. F. F. Lange, "Stress-Induced Phase Transformations: Theory of Retention and Fracture Toughness," ONR Rept. No. 6, Contract N00014-77-C-0441 (October 1979).
4. R. C. Garvie, R. H. Hennick, and R. T. Pascoe, Nature 258, 703 (1975).
5. R. C. Garvie and R. T. Pascoe, Processing of Crystalline Ceramics, ed. by H. Palmour III, R. F. Davis and T. M. Hare (Plenum Press, 1978), p. 263.
6. D. L. Porter and A. H. Heuer, J. Am. Ceram. Soc. 60, 183 (1977); ibid. 280 (1977).
7. T. K. Gupta, J. H. Bechtold, R. C. Kuznichi, L. H. Cadoff, and B. R. Rossing, J. Mat. Sci, 12, 2421 (1977).
8. T. K. Gupta, F. F. Lange, and J. H. Bechtold, J. Mat. Sci. 13, 1464 (1978).
9. F. F. Lange, "Research of Microstructurally Developed Toughening Mechanisms in Ceramics. Stress Induced Transformation Toughening, Part 1: Size Effects Associated with Constrained Phase Transformation Thermodynamics," Technical Report No. 8, Rockwell International Science Center (October 1980).
10. F. F. Lange, private communication.
11. B. R. Lawn and T. R. Wilshaw, J. Mat. Sci. 10, 1049 (1975).
12. A. G. Evans and T. R. Wilshaw, Acta Met. 24, 939 (1976)
13. D. A. Shockey and K. C. Dao, "Improved Impact Fracture Resistance in Oxidation-Toughened Si_3N_4-20 vol % ZrO_2," Bull. Am. Cer. Soc., 60, 256-7 (1981).
14. F. F. Lange, "Research of Microstructurally Developed Toughening Mechanisms in Ceramics" ONR Rept. Part 4, No. 8,9,10,11,12, Contract N00014-77-C-0441 (April 1981).

PUBLICATIONS AND REPORTS UNDER THE PRESENT CONTRACT

The following technical reports and publications resulted from the research performed to date:

D. A. Shockey and Y. M. Gupta,"Impact Erosion Phenomena in Infrared Window and Radome Materials," Semiannual Status Report for Office of Naval Research, Contract N00014-76-C-0657 (November 1976).

D. A. Shockey, D. J. Rowcliffe, and K. C. Dao, "Fracture Toughness of CVD ZnS," Topical Report for Office of Naval Research, Contract N00014-76-C-0657 (March 1977).

D. J. Rowcliffe, R. C. Jones and J. K. Gran, "A Notched-Ring Fracture Toughness Test for Ceramics", Fracture Mechanics of Ceramics Vol. 3 Flaws and Testing, R. C. Bradt, D.P.H. Hasselman and F. F. Lange, Eds., (Plenum Press, New York and London, 1978), pp. 473-482.

D. A. Shockey, Y. M. Gupta, and K. C. Dao, "Production of Cracks in ZnS Under a Uniform Dynamic Stress Field," Annual Report Part I for Office of Naval Research, Contract N00014-76-C-0657 (January 1979).

D. A. Shockey, K. C. Dao, L. Seaman, and D. R. Curran, "Nucleation and Growth of Cracks in CVD ZnS Under Particle Impact," Annual Report Part II for Office of Naval Research, Contract N00014-76-C-0657 (April 1979).

K. C. Dao, D. A. Shockey, L. Seaman, D. R. Curran, and D. J. Rowcliffe, "Particle Impact Damage in Si_3N_4," Annual Report Part III for Office of Naval Research, Contract N00014-76-C-0657 (May 1979).

D. A. Shockey and K. C. Dao, "Improved Impact Fracture Resistance in Oxidation Toughened Si_3N_4 20 vol% ZrO_2," Technical Report to Office of Naval Research, Contract N00014-76-C-0657 (December 1979).

D. A. Shockey and K. C. Dao, "Improved Impact Fracture Resistance in Oxidiation-toughened Si_3N_4 20 vol% ZrO_2," Bulletin of the American Ceramic Society, Vol. 60, No. 2 pp. 256-7 (1981).

D. A. Shockey, D. C. Erlich, and K. C. Dao, "Particle Impact Damage in Silicon Nitride at 1400°C," Journal of Materials Science, 16 pp. 77-82 (1981).

D. A. Shockey, "Particle Impact Damage in Ceramics", Annual Report--Part IV for Office of Naval Research, Contract N00014-76-C-0657 (March 1981).

J. H. Giovanola and D. A. Shockey, "Particle Impact Damage in Ceramics", Final Annual Report to Office of Naval Research, Contract N00014-76-C-0657 (April 1981).

J. H. Giovanola and D. A. Shockey, "Impact Resistance of $Al_2O_3 \cdot ZrO_2$ Composite Ceramics" to be published in Proceedings of International Symposium on the Fracture Mechanics of Ceramics, Penn State University, July 15-17, 1981 .